

# Biomechanics of Aortic Wall Failure with a Focus on Dissection and Aneurysm: A Review

Selda Sherifova<sup>a</sup>, Gerhard A. Holzapfel<sup>a,b,\*</sup>

<sup>a</sup>*Institute of Biomechanics, Graz University of Technology, Stremayrgasse 16/2, 8010 Graz, Austria*

<sup>b</sup>*Department of Structural Engineering, Norwegian Institute of Science and Technology (NTNU)  
7491 Trondheim, Norway*

---

## Abstract

Aortic dissections and aortic aneurysms are fatal events characterized by structural changes to the aortic wall. The maximum diameter criterion, typically used for aneurysm rupture risk estimations, has been challenged by more sophisticated biomechanically motivated models in the past. Although these models are very helpful for the clinicians in decision-making, they do not attempt to capture material failure. Following a short overview of the microstructure of the aorta, we analyze the failure mechanisms involved in the dissection and rupture by considering also traumatic rupture. We continue with a literature review of experimental studies relevant to quantify tissue strength. More specifically, we summarize more extensively uniaxial tensile, bulge inflation and peeling tests, and we also specify trouser, direct tension and in-plane shear tests. Finally we analyze biomechanically motivated models to predict rupture risk. Based on the findings of the reviewed studies and the rather large variations in tissue strength, we propose that an appropriate material failure criterion for aortic tissues should also reflect the microstructure in order to be effective.

*Keywords:* aortic dissection, aortic aneurysm, aortic failure, aortic microstructure, tissue strength, uniaxial tensile test, bulge inflation test, peeling test, rupture risk

---

---

\*Corresponding author

Email address: holzapfel@tugraz.at (Gerhard A. Holzapfel)

## 1. Introduction

Aortic dissection and aortic aneurysm rupture are acute life threatening events. Overall mortality rates of dissections and aneurysms of the thoracic aorta remain high despite the improvements over the years (Olsson et al., 2006; Svensson et al., 2008; Pape et al., 2015). Ruptured aneurysms of the abdominal aorta are estimated to cause 4–5% of sudden deaths in the United States, and the event of rupture has mortality rates as high as 80% (Schermerhorn, 2009).

Aortic dissection is an acute condition of the aorta which typically starts with an intimal tear to the presumably already weakened wall, followed by a crack in the radial direction. The crack then proceeds within the medial layer, or between the media and the adventitia, causing the layers of the aortic wall to separate, thereby creating a false lumen where the blood can flow into (Mikich, 2003; Jameson et al., 2018). This leads to a dilatation and a further weakening of the intact outer wall of the false lumen. In most fatal conditions, the aorta bursts causing the patient to bleed to death quickly (Oberwalder, 2001; Criado, 2011). Stanford type A dissections – affecting the ascending aorta – are shown to become chronic only rarely, whereas type B dissections – affecting the descending thoracic aorta only – are routinely chronic with a thickened, straightened intimal flap which lost its mobility due to remodeling (Peterss et al., 2016). Approximately 67% of the cases are reported to be type A dissections (Pape et al., 2015). The risk factors include but are not limited to age, hypertension, smoking, congenital disorders such as bicuspid aortic valve (BAV), genetic disorders such as Marfan syndrome and Ehlers-Danlos syndrome (Isselbacher, 2005; Elefteriades, 2008). Intimal tears leading to ascending aortic dissection are typically located a few centimeters above the coronary arteries, whereas the ones leading to descending aortic dissection are located a few centimeters beyond the left subclavian artery (Elefteriades, 2008). For a mechanical assessment of arterial dissections see the review article by Tong et al. (2016). Figure 1(a) illustrates the basic anatomy of the aorta, while the sketch in Fig. 1(b) shows a dissected wall with arrows indicating the blood flow.

Aortic aneurysms are local dilatations of the aorta, typically more than 50% of the normal diameter (Goldfinger et al., 2014). The underlying mechanisms leading to aneurysm formation differ between the ascending aorta and the descending thoracic aorta (Saeyeldin et al., 2017), as

well as between the thoracic and the abdominal aorta (Elefteriades, 2008; Ruddy et al., 2013; 30 Cherif et al., 2015) due to different embryonic origins of the cells involved in the remodeling process. The aneurysms in the ascending aorta are usually not accompanied by atherosclerosis, whereas in the descending thoracic and the abdominal aorta it is a common finding (Isselbacher, 2005). Nevertheless, all aneurysms are characterized by alterations to the extracellular matrix. For a review on the biomechanics, mechanobiology, and modeling of aneurysms see Humphrey 35 & Holzapfel (2012).

In addition to the above mentioned pathologies, thoracic aortic trauma is accountable for a large percentage of losses involving motor vehicle accidents, and it can initiate the dissection process or cause an immediate rupture. Bertrand et al. (2008) reported 1.2% of the occupants involved in vehicular accidents sustained a traumatic injury of the aorta, of which 94% were 40 deadly, accounting for 21.4% of all fatalities. Traumatic aortic injury can also be due to heavy falls on feet, airplane crashes, suicide attempts, or surgical procedures (Henson & Rob, 1956; Sevitt, 1977; Harvey & Gough, 1981). The ascending aorta is reported to be the most common injury site due to trauma (Marshall, 1958), whereas the aortic isthmus has been identified as the most vulnerable location for injury by several studies (Creasy et al., 1997; Shkrum et al., 1999; 45 Bertrand et al., 2008) constituting a number as high as 90% (Creasy et al., 1997), followed by the aortic arch and the abdominal aorta around the bifurcations.

To prevent further complications such as rupture, dilatations of the aorta due to aneurysm or aortic dissection are surgically treated if the maximum diameter of the lesion is above 5.0 cm in women or 5.5 cm in men, or if the maximal diameter increases more than 0.51 cm in one year 50 (Lederle et al., 2002; Hans et al., 2005; Grootenboer et al., 2009). Clinicians consider several indicators before decision-making about a surgical intervention – such indicators include maximum diameter, expansion rate, genetic risk factors and the family history just to name a few. For example, the maximum diameter criterion is revised if the patient suffers from a connective tissue disorder such as Marfan syndrome, see Brownstein et al. (2018), and Fig. 1 therein. 55 Even though it has been shown that the risk of rupture and dissection of aneurysms increase significantly at sizes larger than 6 cm for the thoracic aorta (Davies et al., 2002), this criterion

is in contradiction with the observation that aneurysms can rupture or dissect at any diameter (Campa et al., 1987; Pape et al., 2007; Vorp, 2007; Pape et al., 2015; Saeyeldin et al., 2017), and it ignores the more complex relationships between the rupture and the material properties such as the heterogeneity of tensile strength in the wall of aortic aneurysms (Vallabhaneni et al., 2004). Clinicians need more reliable tools to assess the risk of intervention versus the risk of rupture, as the maximum diameter criterion can underestimate the rupture risk of smaller aneurysms, and overestimate it for the larger ones.

To gain a more in-depth understanding of the possible mechanisms leading to these fatal events, this review analyzes experimental studies that aim to quantify the strength of aortic walls towards a material failure perspective and reviews biomechanically motivated models to predict rupture risk. After summarizing the microstructure of the aorta in Section 2, we continue with a brief account of damage and failure mechanisms involved in the dissection and rupture in Section 3. Subsequently, in Section 4 we summarize some important experimental studies that quantify the strength, and in Section 5 we summarize the state-of-the-art on the biomechanics-based rupture risk prediction models for clinical use. Finally, within Section 6, we provide concluding remarks. Readers interested in damage models or computational aspects of failure are referred to, e.g., the two recent book chapters of Holzapfel & Fereidoonzhad (2017) and Gültekin & Holzapfel (2018), respectively.

## 2. Microstructure

We continue with a glance at the structure of the aorta as it provides a basis for our discussion. The aorta is composed of the intima, media and adventitia, as shown in Fig. 2(a). The intima is mechanically negligible in a young and healthy aorta, and it is basically a single layer of endothelial cells (Holzapfel et al., 2000). This layer becomes mechanically significant, especially with age, due to non-atherosclerotic intimal thickening during which collagen fibers are deposited (Canham et al., 1989). Figure. 2(a) shows a sketch of such an artery with intimal thickening, while Fig. 2(b) partly depicts the collagen architecture of a healthy (but aged) wall obtained from an abdominal aorta and produced with second-harmonic generation microscopy.

The media consists of several concentric lamellar units bound together, see Fig. 2(a),(c). Each  
85 of these units contains smooth muscle cells with their radially tilted longer axes oriented at an  
angle closer to the circumferential direction, surrounded by collagen fibers embedded in the ex-  
tracellular matrix (O’Connell et al., 2008), see Fig. 2(c),(d). Collagen in the media is typically  
present as two symmetric families of fibers with a mean orientation closer to the circumferential  
direction, whereas in the adventitia the mean orientation is closer to the longitudinal direction  
90 (Schriebl et al., 2012). The media is the main load bearing layer for physiological loads, and  
the adventitia acts as a stiff jacket-like tube at higher levels of pressure, which prevents the  
artery from overstretch and rupture (Holzapfel et al., 2000). The thickness of the thoracic aortic  
media go hand in hand with an increase in the number of lamellar units, and the thickness of  
a single lamellar unit is constant amongst mammalian species (approximately  $15\ \mu\text{m}$ ) (Wolin-  
95 sky & Glagov, 1967, 1969). However, human abdominal aortas have fewer lamellae for a given  
thickness compared to other species (Wolinsky & Glagov, 1969). Growth of the human thoracic  
aorta is thought to be primarily due to the increase in the number of lamellar units, whereas in  
the human abdominal aorta it is mainly due to the increase in the thickness of the lamellar units  
(Wolinsky, 1970).

100 A key structural change in thoracic aortic dissections is the so-called medial degeneration,  
as first reported by Erdheim (1929). Typically, it involves smooth muscle cell loss, elastic fiber  
fragmentation, and an accumulation of proteoglycans (Borges et al., 2009; Bode-Jänisch et al.,  
2012; Wu et al., 2013). A weakened aortic wall due to medial degeneration is also typical  
for aneurysms and dissecting aneurysms of the ascending aorta (Borges et al., 2014), not only  
105 with tricuspid aortic valve (TAV) but also with BAV and bovine aortic arch phenotypes (Pham  
et al., 2013), see Fig. 3(a)–(f) for examples of proteoglycan accumulation zones. Versican and  
aggrecan were identified as the major components of such accumulations in thoracic aortic  
aneurysm and dissection patients (Cikach et al., 2018). In addition, one can see a change in  
the elastic fiber structure of a dissected aorta (Fig. 3(g)) where the elastic structure connecting  
110 the lamellar units are highly degenerated compared to a control aorta (Fig. 3(h)) (Nakashima,  
2010). Collagen content has been reported to increase (Wang et al., 2006; Cheuk & Cheng,

2011; Wang et al., 2012) or decrease with an increased disruption (Borges et al., 2008, 2014) for aortic dissections.

Dilatation of the aortic wall secondary to disruptions in elastin organization was reported in a mice study (Jones et al., 2009). Although elastin content in the thoracic aortas of patients with an ascending aneurysm (TAV and BAV) decreased compared with control, it was not significantly different between BAV and TAV groups (Choudhury et al., 2009; Deveja et al., 2018). In addition, changes in the elastin architecture of BAV patients compared with TAV were region-specific, and were characterized by a decrease in the number of radially oriented elastin fibers (Tsamis et al., 2016). Primary elastin fiber orientation in the aneurysmatic media of TAV patients changed from longitudinal in the inner part to circumferential in the outer part distinctly in the right lateral region compared with other regions (Sokolis et al., 2012a).

Similar collagen levels were observed between control and ascending aneurysm samples (Jones et al., 2009; Kritharis et al., 2014; Deveja et al., 2018), and between BAV and TAV phenotypes (Pichamuthu et al., 2013; Phillippi et al., 2014; Deveja et al., 2018) contradicting the findings of significantly higher collagen in BAV compared with TAV and control (Choudhury et al., 2009). Regardless, the organization of collagen may still be significantly changed during aneurysm development in the thoracic aorta (Borges et al., 2008). Sassani et al. (2015) reported notable regional variations in the 2D collagen orientation, with the right lateral and posterior regions having diagonal fibers at smaller angles to the longitudinal axis. On the other hand, Forsell et al. (2014) reported similar collagen orientations in aneurysmatic BAV and TAV groups. Phillippi et al. (2014) demonstrated that both collagen and elastin fibers in the tangential plane were more aligned in BAV aneurysms and BAV control, and more disorganized in TAV aneurysms compared with TAV control. Percentage of radially oriented elastin and collagen fibers in the outer media was significantly higher in BAV patients and higher in TAV patients compared with control (Tsamis et al., 2013).

Abdominal aortic aneurysms (AAAs) typically show increased collagen synthesis at earlier stages, whereas later in the process collagen degradation exceeds its synthesis, and it is accompanied by elastin degradation (Shimizu et al., 2006). The out-of-plane collagen dispersion in

140 AAAs is significantly higher when compared with abdominal aortic tissues, and the characteristic wall structure (with three distinct layers) cannot be identified anymore in AAA samples. In addition, collagen fibers in the abluminal layer of AAAs lose their waviness and appear as thick straight struts (Niestrawska et al., 2016).

Several factors in the donor anamnesis may have an influence on the microstructure making it difficult to conclude, for example, which disease is accompanied with which structural changes and at which stages. Nevertheless, the microstructure remains a crucial contributor to mathematical models if one wishes to describe the mechanics and failure.

### 3. Failure Mechanisms Involved in Dissection and Rupture

We now study the load combinations that act on the tissues *in vivo* prior to dissection and 150 rupture, which should be taken care of for a better understanding of tissue failure. In Section 3.1 we start with different theories regarding the loading conditions initiating and propagating the aortic dissections, and continue in Section 3.2 with theories regarding the global and local loading conditions prior to rupture in vehicular trauma. As we will see in the following sections, different loading conditions may lead to similar tissue failure.

#### 155 3.1. Initiation and propagation of aortic dissection

The study of van Baardwijk & Roach (1987) applied pulse pressure to canine thoracic aortas after creating an intimal tear. The authors identified the maximum rate of pressure change  $(dP/dt)_{\max}$  as the most clearly linked parameter to the propagation of dissection since the crack advanced at the upstroke of the pulse wave. Gaps between the lamellae, as identified during 160 histological investigations, pointed to shearing mechanisms that are responsible for the crack propagation, and the crack typically propagated between adjacent elastic layers. The dissection rate was variable between the pulses, and it was inversely related to the tear depth within the medial layer in contrast to expectations, suggesting heterogeneous wall properties throughout the thickness.

165 On the other hand, Carson & Roach (1990) reported that the medial strength of the porcine aortas does not change with depth under static pressure. The authors stated that the structures

linking the lamellae are weaker than the lamellae themselves, resulting in a crack propagation between the lamellae. In addition, the fusion points of the lamellae can force the crack to change the direction. The authors reported quite high pressure values to initiate a bleb, but observed a quick drop in the pressure allowing the dissection to propagate under a physiological load level. A minimum pressure value required for the crack to propagate was not reported therein. Using similar methods to Carson & Roach (1990), Tiessen & Roach (1993) reported similar results regarding the effect of the tear depth for human aortas, however, the authors noted that the dissection propagated around the plaques instead of going through them. The experiments on porcine aortas performed by Roach & Song (1994) showed that although it was much easier to initiate a dissection in the abdominal aorta when compared to the thoracic aorta, the dissections propagated more easily in the thoracic aorta, see Fig. 4. The authors suggested that this is because of structural differences in the elastin pattern between the two sections of the aorta; parallel sheets with fenestrations in the thoracic aorta and a honeycomb-like structure in the abdominal aorta. In a later study, Tam et al. (1998) reported that the dissection closer to the adventitial side required a lower pressure to propagate.

The study of Rajagopal et al. (2007) suggested hemodynamics together with abnormal mechanical properties, geometry, and the anisotropic wall structure to be important factors for the initiation and the propagation of aortic dissections. The authors proposed that an increased maximum systolic pressure and the mean aortic blood pressure are responsible for the initiation, and an elevated pulse pressure and the heart rate facilitate the propagation. Mikich (2003) proposed that the blood flow and the hemorrhage in the media alone cannot cause an initiation and propagation of a dissection, but the process is mainly influenced by smooth muscle cell contraction.

Haslach, Jr. et al. (2011) proposed that collagen fiber pullout, during which bonds and filaments attached to the fibers rupture due to shear, is a prerequisite for rupture in circumferential aortic tensile strips and inflated ring specimens. For the longitudinal tensile strips, however, rupture is caused by a peeling mechanism during which the bonds between collagen fibers and the ground matrix rupture. In addition, hydration of the tissue is suggested to play an important

195 role to recover from permanent deformation, loss of which eventually leads to rupture. This re-  
search group conducted more ring inflation tests, see Haslach, Jr. et al. (2015, 2018), concluding  
that, as a result of heterogeneous circumferential deformation, non-negligible circumferential  
shear stresses could be the reason for the crack propagation in the circumferential–longitudinal  
plane considering the lamellar structure of the media. Histological investigations of block shear  
200 tests showed voids between the collagen bundles, see Fig. 5(a)–(c), possibly resulting from  
the relative motion of the layers, which can be an indicator of ruptured inter-fiber cross-links  
(Haslach, Jr. et al., 2015). Sommer et al. (2016) reported similar observations within in-plane  
shear tests, as shown in Fig. 5(d), and this mechanism could explain the delaminations observed  
by Helfenstein-Didier et al. (2018) during uniaxial tensile tests, as depicted in Fig. 5(e).

205 Following the protocol reported by Sugita & Matsumoto (2013b), recently Sugita & Mat-  
sumoto (2018) performed biaxial extension tests on thinly sliced porcine thoracic aortas with a  
reduced cross section in the center and reported a heterogeneous deformation field in terms of  
strains similar to Sugita & Matsumoto (2013a). Strain distribution and the collagen realignment  
were similar between the crack initiation sites and the remaining tissue sample, in contrast to  
210 the idea behind the maximum principal strain failure criterion. Since the collagen density was  
significantly lower at the crack initiation sites and the cracks propagated along the local collagen  
fiber direction, the authors suggested that the initiation and propagation of the crack is primarily  
effected by the collagen architecture. However, anticipated crack initiation at the lowest retar-  
dance sites – in other words the sites with the least collagen content – was not observed for all  
215 specimens. This suggests that the cross-links between the fibers might also play an important  
role in the dissection process.

Considering the changes to elastic fibers in aortic dissections and their role in energy dissi-  
pation, Chung et al. (2014) studied elastic energy loss, defined as the hysteresis divided by the  
total strain energy. The authors found that an increased elastic energy loss is associated with  
220 medial degeneration and with increased collagen to elastin ratio. Furthermore, Chung et al.  
(2017) reported a decrease in the directional differences in energy loss – hence in the degree  
of anisotropy – in samples with severe medial degeneration. By using newborn mice and ge-

netic engineering to have defects in the elastic fiber structure, Kim et al. (2017) suggested that not only elastin but properly assembled and cross-linked elastic fibers are responsible for a low energy loss in the aorta.

### 3.2. Traumatic rupture

Blunt aortic trauma typically constitutes a transverse tear in the aortic wall, rarely a longitudinal one (see Fig. 6(a)). The mild degree trauma involves an intramural rupture (laceration), typically leading to a traumatic aortic dissection initiated by a circumferential tear to the intima, which may propagate and lead to complete rupture later in life (Keen, 1972; Prijon & Ermenc, 2010). Severe trauma involves a transmural injury to the aortic wall, which can be in the form of partial, complete, or multiple transections. Figure 6(b)–(c) shows examples of intramural ruptures with different extents. Multiple ruptures as a combination of intramural and transmural ruptures are also reported in the literature (Soyer et al., 1992; Creasy et al., 1997).

One of the first mechanisms proposed to explain traumatic rupture was the sudden increase in the intraluminal pressure. For example, the shoveling effect – the heart being trapped between the vertebral column, the sternum and the mediastinum due to the compression of the chest and the abdomen – can force the blood from the heart into the aorta suddenly increasing the intraluminal blood pressure (Ben-Menachem & Handel, 1981). The effect of this pressure increase can be elevated by the cardiac cycle in different ways. For example, Wilson & Roome (1933) hypothesized that the aorta is more likely to rupture if an impact to the chest is received at the beginning of diastole since the aorta is completely filled with blood, whereas Marsh & Moore (1957) suggested that the deceleration forces acting on the heart during the systole creates a greater risk of rupture of the great vessels at the location of their attachment to the heart. In addition, a phenomenon known as water hammer effect might occur due to the sudden deceleration of the blood in the arch impacting the anterior wall of the aorta and resulting in traction forces on the isthmus region (Kivity & Collins, 1974; Shkrum et al., 1999). The occlusion of the aortic lumen due viscoelastic effects that decrease the aortic diameter can cause formation of shock waves propagating in the counter-blood flow direction, thereby exerting high axial stresses on the aortic wall and causing a transverse rupture (Kivity & Collins, 1974).

In addition to the hemodynamic effects, local concentrations of shear stresses may arise due to high deceleration forces (Greendyke, 1966), the rotation of the first ribs (Crass et al., 1990), or a combination of rapid deceleration and chest compression (Shkrum et al., 1999). Vertical inertial forces (Zehnder, 1956), rapid deceleration occurring at different rates at different parts of the body (Marsh & Moore, 1957; Crass et al., 1990; Shkrum et al., 1999), cranial deceleration (Sevitt, 1977), the heart being displaced in the thoracic cavity due to inertial effects (Viano, 1983) and the displacement of mediastinal structures (Shkrum et al., 1999) can all cause stretching of the aortic wall between fixation points resulting in an injury to the isthmus area due to stress concentrations. Field et al. (2007) suggested that traumatic injury does not necessarily follow along the luminal/abluminal direction, considering that some patients did not present an intimal flap. The authors hypothesized that the geometry of the isthmus region in combination with the high number of small branching vessels lead to stress concentrations which are naturally occurring, and the stretching of these vessels may pronounce the effect of inertial or compressive chest loading resulting in intimal rupture, or intramural hematoma.

The above mentioned mechanisms for initiation and propagation of dissection as well as traumatic aortic injury indicate that the cardiac cycle, the blood flow and the geometry of the aorta together with the aortic attachment points are important factors to consider as they influence the boundary conditions to be imposed on the problem.

#### **4. Tissue Strength Quantification**

Aneurysms rupture when the wall stress exceeds the wall strength. Although it sounds simple, the requirement here is to reliably characterize both the (*in vivo*) stress state of the wall and the (*in vivo*) tissue strength, and neither is trivial. It is inarguably valuable to know how the aortic wall behaves under different loading modes – separated and mixed – to be able to predict the stress state of the wall. However, how much of the stress the tissue can bear at certain loading conditions with a given state of the microstructure remains unknown. As an essential element to a failure criterion framework, the strength quantification needs to be addressed. In this section, we provide an overview of the documented experimental studies quantifying the

strength of the aorta in health and disease. We review uniaxial tensile tests performed until failure, bulge inflation and peeling tests and (roughly) summarize related data in the Tables 1–  
280 3, respectively. Finally we describe other tests quantifying the tissue strength such as in-plane shear, direct tension and trouser tests. For an illustration of the different tests used to quantify failure properties of aortas see Fig. 7.

#### 4.1. Uniaxial tensile tests performed until rupture

Uniaxial tensile tests have been widely employed to characterize the mechanical properties  
285 of aortic tissues. Because of the anisotropic microstructure of the aortic wall, they are typically performed in circumferential and longitudinal directions to obtain direction-dependent properties. The shape of the specimen is either rectangular or (better) bone-shaped, as shown in Fig. 7(a). Table 1 summarizes some of the studies documented in the literature and provides failure stress and stretch values under uniaxial tensile loading. This table is not meant to be a  
290 complete summary of all uniaxial rupture tests published in the literature, however, it aims to provide a representative overview and points to the rather large variability in the failure stress and stretch values, also visualized in Fig. 8.

In terms of failure stress the thoracic aortic tissue has been reported to be stronger in the circumferential direction than in the longitudinal direction (Mohan & Melvin, 1982; Iliopoulos  
295 et al., 2009b; García-Herrera et al., 2012; Pichamuthu et al., 2013; Shah et al., 2014; Ferrara et al., 2016; Sommer et al., 2016). However, Vorp et al. (2003) observed no significant differences in regard to the testing direction. The study of Mohan & Melvin (1982) stated that the longitudinal aortic strength should be more than twice as high as the circumferential strength for the transverse failure to occur. Their quasi-static tests showed no such difference, however,  
300 once the strain rates were increased the strength ratios got closer to 1:2. The extension ratios were not effected by the strain rate.

In terms of the ‘yield stress’ the anterior region of AAAs was reported to be the weakest, especially along the longitudinal direction (Thubrikar et al., 2001) – ‘yield stress’ is here related to the yield point defined as the point on the stress-strain curve where the slope starts to decrease  
305 with increasing strain. Failure stresses of anterior, right lateral, posterior and left lateral samples

of the ascending aortas were not significantly different for control (Iliopoulos et al., 2009b), for aneurysmatic (Iliopoulos et al., 2009a,b), and for dissected tissues (Manopoulos et al., 2018) with respect to the circumferential direction. However, failure stresses in the longitudinal direction were significantly higher in the right lateral region compared with the anterior and posterior regions (Iliopoulos et al., 2009b), but also in the left and right lateral regions compared with the anterior region for aneurysms (Iliopoulos et al., 2009a); and in the right lateral region compared with the left lateral region for dissections (Manopoulos et al., 2018). Ferrara et al. (2016) reported stronger and stiffer posterior regions with respect to anterior in the circumferential direction for thoracic aortic aneurysms, whereas the opposite trend was observed for the longitudinal direction. Kritharis et al. (2014) found similar failure properties in the noncoronary sinuses of the control and aneurysm groups for both young and old patients, whereas failure stresses in the right and left coronary sinus regions were smaller circumferentially and greater longitudinally in aneurysms compared with control.

Although all three layers of ascending thoracic aortic aneurysms exhibited higher failure stresses in the circumferential direction than in the longitudinal direction, the differences were significant only for the media from all regions and for the adventitia from the lateral region (Sokolis et al., 2012b). For dissected tissues, failure stresses and stretches were significantly higher in the circumferential than in the longitudinal direction in the inner media at the distal location, but the outer media did not show significant differences regarding the testing direction (Manopoulos et al., 2018). Failure stretches of the ascending tissue did not show notable differences between the layers (Sokolis et al., 2012b; Manopoulos et al., 2018). However, failure stresses were significantly higher for the adventitia than for the media and intima for aneurysms (Sokolis et al., 2012b), and they were significantly higher for the outer media than for the inner media for dissections (Manopoulos et al., 2018).

Healthy abdominal aortic tissues had significantly higher ultimate strength and yield strength compared to AAAs (Raghavan et al., 1996). Failure tension (for definition see Raghavan et al. (2006)) was suggested to be a better predictor of strength than failure stress (Raghavan et al., 2006), however, no significant differences were found between ruptured and unruptured AAAs

in terms of either parameter (Raghavan et al., 2011). In contrast, circumferential strips of rup-  
335 tured AAA tissues were reported to have significantly lower failure stresses compared with the  
unruptured AAA tissue strips by Di Martino et al. (2006). Vorp et al. (1996) reported isotropic  
failure properties for orthogonal strips taken from abdominal aortic aneurysms. Moreover, the  
failure stress in the longitudinal direction was significantly lower for AAA compared with con-  
trol. Partially calcified AAA tissue was significantly weaker than the fibrous AAA tissue in  
340 terms of the failure stress, stretch and tension (O’Leary et al., 2015). Failure stresses of the  
AAA wall were also reported to decrease with increasing intraluminal thrombus (ILT) thickness  
(Vorp et al., 2001; Martufi et al., 2015).

Vorp et al. (2003) reported aneurysmatic ascending aortas to have significantly lower failure  
stresses and stiffer behavior compared to controls. García-Herrera et al. (2012) documented  
345 no significant differences between the mechanical strength of aneurysmal BAV and aneurys-  
mal TAV aortic specimens, and the corresponding age-matched control group for the ascending  
aorta. Significantly higher failure stresses were reported in aneurysmatic BAV ascending aortas  
when compared to aneurysmatic TAV ascending aortas for the intact wall (Pham et al., 2013;  
Pichamuthu et al., 2013; Forsell et al., 2014; Deveja et al., 2018; Ferrara et al., 2018), and for the  
350 media (Deveja et al., 2018). The failure stretches in two valve phenotypes were similar (Pham  
et al., 2013; Forsell et al., 2014), but also significantly higher for BAV than for TAV (Deveja  
et al., 2018; Ferrara et al., 2018). Histological investigations showed that proportional differ-  
ences in the tensile strength between BAV and TAV groups cannot be explained by alterations  
in the elastin content (Deveja et al., 2018) or the collagen content (Pichamuthu et al., 2013;  
355 Deveja et al., 2018). However, the stiffness increase and extensibility reduction in ascending  
aneurysmatic tissues were associated with a decreased elastin content (Sokolis et al., 2012a).

In the study of Vande Geest et al. (2006a) no statistically significant gender-related differ-  
ences were reported in terms of strength, unlike Sokolis & Iliopoulos (2014) who identified that  
circumferential aneurysmatic specimens obtained from female patients exhibited significantly  
360 lower failure stresses compared with the ones obtained from male patients. Furthermore, failure  
stresses of the aorta are reported to decrease (Okamoto et al., 2002; García-Herrera et al., 2012;

Kritharis et al., 2014; Ferrara et al., 2018), and also the failure stretches (Okamoto et al., 2002; Kritharis et al., 2014; Ferrara et al., 2018) with increasing age. In general, strength was not correlated to diameter (Di Martino et al., 2006; Iliopoulos et al., 2009a), but it was inversely related  
365 to wall thickness (Thubrikar et al., 2001; Di Martino et al., 2006; Iliopoulos et al., 2009a).

#### 4.2. Bulge inflation tests

Although uniaxial tensile tests provide valuable insight into the strength characteristics of aortic tissues, they are limited when it comes to representing *in vivo* loading conditions. Methods to quantify tissue strength using planar biaxial tests are not yet developed to the authors' knowledge, therefore, biaxial tests performed via a bulge inflation method, see Fig. 7(b), are the  
370 focus of this section. Table 2 summarizes some studies documenting failure stress and (when available) extension to failure, defined in various ways (see the related table).

Aortic specimens failed consistently in the direction perpendicular to the longitudinal axis in bulge inflation tests for human (Mohan & Melvin, 1983) and for porcine tissue (Marra et al.,  
375 2006), and the dynamic biaxial failure pressure was significantly higher than the quasi-static one, 2.14 times (Mohan & Melvin, 1983). Sugita et al. (2012) also documented the normal aorta to be weakest in the longitudinal direction under bulge inflation tests, but there was no dominant crack direction for the aneurysmal tissues. The authors did not observe a persistent rupture initiation at local strain concentration zones in contrast to Kim et al. (2012) who reported  
380 local strain and stress concentrations at the rupture locations. The study of Kim et al. (2012) deduced a stable stress parameter for rupture, quantifying the stress in the direction normal to both families of collagen fibers using the values provided in Table 2. Romo et al. (2014) showed that localized thinning of the wall is responsible for rupture and not the location of maximum stress. The related values in Table 2 are the stresses in the direction perpendicular to the crack  
385 direction at rupture. Duprey et al. (2016) calculated failure stress and stretch similar to Romo et al. (2014). Cracks showed dissection-like properties, where the media and the intima failed first creating a sudden drop in the stress curves, but the adventitia was still able to carry (some) load. The authors found no significant differences between BAV and TAV patients, whereas age had a significant impact on the failure properties. In addition, they reported no correlation

390 between the aneurysm diameter and the failure stress/stretch. Luo et al. (2016) investigated the elastic properties, direction of maximum stiffness, stress, strain, and the energy consumption at the rupture sites of 9 aneurysmatic ascending aortic samples. The authors reported the tissues to consistently fail in the direction of maximum stiffness and highest energy, indicating that higher stiffness does not mean higher strength. Since high stiffness and energy values mean  
395 more collagen recruitment, they concluded that collagen fibers must play a significant role in the rupture process.

Pearson et al. (2008) found no significant differences in rupture pressure between the ascending, descending, and isthmus regions. However, they reported significantly larger extension to failure in the ascending aortic samples compared to the isthmus samples, which is in  
400 contrast to Marra et al. (2006) who found no significant influence of the aortic location on the axial failure stress or stretch. Histological investigations in Pearson et al. (2008) showed isthmus samples to have a higher collagen to elastin ratio, likely making the samples from this region less extensible. The failure stresses were significantly larger for the descending aorta than for the isthmus region, however, the overlap in the data between the isthmus and the adjacent  
405 regions let the authors conclude that the mechanical failure properties cannot account for the clinical observations pointing to the isthmus as a primary injury location.

### 4.3. Peeling tests

As mentioned above, the propagation of the dissection is mainly attributed to the lamellar structure of the aortic wall. Peeling tests, which is not the sole appropriate method, can provide  
410 us with the delamination strength of the wall at different locations. The ‘strength’ of the wall is typically quantified in terms of force per width ( $F/w$ ) and the dissection energy ( $W_{\text{diss}}$ ). On the basis of some studies Table 3 provides an overview of these values for the aorta, and Fig. 7(c) shows a sketch of a peeling test.

Higher force per width for axial strips compared to circumferential strips of the abdominal  
415 aortic media was reported by Sommer et al. (2008) – note that this difference was not significant. Furthermore, the authors observed that the damage was spread over six to seven lamellae. Figure 9(a),(b) depicts the histological sections of circumferential and longitudinal strips under

peeling. Pasta et al. (2012) investigated the dissection properties of human ascending aortas in aneurysmal BAV and TAV patients. Compared to the control group, both aneurysm groups  
420 required significantly lower force per width, where the TAV group was significantly stronger than the BAV group. The controls showed a strong anisotropy, where the axial direction was significantly stronger, which was not observed in neither aneurysm group. Scanning electron microscopy investigation showed a larger number of ruptured elastin fibers, which is in accordance with the fiber bridging failure mode, see Fig. 9(c).

425 Kozuń (2016) showed that the dissection properties are direction dependent also for stage II atherosclerotic aortas (classification according to Stry (2003)), in particular the force per width  $F/W$  and the dissection energy  $W_{\text{diss}}$  were higher in the longitudinal direction. In addition, a significantly higher dissection energy  $W_{\text{diss}}$  for the adventitia/media + intima (A-MI) interface compared to the adventitia + media/intima (AM-I) interface was reported. Following  
430 Kozuń (2016), Kozuń et al. (2018) found the dissection energy for A-MI and AM-I interfaces in both circumferential and longitudinal directions to decrease with later stages of atherosclerosis (classification according to Stry (2003)) until stage IV, whereas stages V and VI were characterized by an increase in the energy. Tong et al. (2014) reported a decreased dissection energy for the media/intima (MI) composite as well as a decreased anisotropy with increasing  
435 ILT age. In addition to the values provided in Table 3, the authors performed peeling tests on the ILT. Histological investigations showed smooth peeling surfaces in the ILT due to single fibrin fibers or smaller protein clots within the ILT. In addition, the elastin content in the wall decreased as the thrombus age increased, whereas the collagen content did not change significantly. The authors reported a rate-dependent change in the dissection properties of both the ILT  
440 and the ILT-covered wall. Noble et al. (2016) analyzed the influence of collagenase, elastase, and glutaraldehyde treatment on the dissection properties of porcine thoracic aortas. Collagenase significantly decreased the resistance to dissection, whereas glutaraldehyde increased it and elastase had no significant effect. In terms of anisotropy, their results were similar to Sommer et al. (2008).

445 *4.4. Other tests quantifying tissue strength*

Trouser tests, as illustrated in Fig. 7(d), in addition to uniaxial tensile tests, were performed on porcine descending thoracic aortas by Purslow (1983). The author reported that the longitudinal direction is more resistant to tearing than the circumferential direction, such that some longitudinal test samples showed cracks that deviated to the circumferential direction making data from these tests unusable for further analysis. In addition, the author found that the circumferential toughness increased with increasing distance from the heart. The study of Chu et al. (2013) showed that the stiffness and the fracture toughness of aortas decreased with increasing fatigue by using cyclic loading tests followed by biaxial and guillotine tests. On the basis of the guillotine method documented by Chu et al. (2013), Shahmansouri et al. (2016) used a custom-made toughness-tester apparatus for tests on control and aneurysmatic ascending aortic tissues taken from four quadrants, and the authors measured the circumferential toughness and the incremental elastic modulus at 10% Green-Lagrange strain. Neither parameter showed regional dependency, however, both correlated well with the total amount of structural proteins (collagen and elastin). More specifically, the toughness decreased with increasing collagen content. The average toughness was not correlated with the average circumferential or longitudinal moduli.

Curves of direct tension tests (see Fig. 7(e)) on abdominal aortas (Sommer et al., 2008) and thoracic aortas (Sommer et al., 2016) showed three characteristic regions, namely elastic, damage, and failure. The average radial failure stress for human abdominal aortas was  $140.1 \pm 15.9$  kPa and for diseased human thoracic aortas  $131 \pm 56$  kPa. Comparing these values with the data from uniaxial tests in Table 1, it is clear that the aorta is weakest in terms of the failure stress under radial loading due to its lamellar structure, as also pointed out by MacLean et al. (1999), see Fig. 2.

In-plane and out-of-plane shear tests until failure in circumferential and longitudinal directions were performed on diseased human thoracic aortas by Sommer et al. (2016). The sheared plane and the direction of shearing during an in-plane shear test is depicted in Fig. 7(f). Out-of-plane shear strength was almost 10-fold higher compared to the in-plane shear strength, which is a result of the lamellar structure and the collagen architecture of the aorta. The shear-lap

test results of Witzenburg et al. (2017) were similar to the in-plane shear tests of Sommer et al. (2016), although the geometry of the samples were slightly different. The authors reported that  
475 circumferential samples exhibited significantly higher peak stresses (nominal) than longitudinal samples.

## 5. Biomechanically Motivated Models to Predict Rupture Risk

There may be different reasons for the similar locations at which traumatic injuries and the initiation of aortic dissections occur, as pointed out in the introduction. One reason may  
480 be that since the aorta is attached to the left pulmonary artery by the ligamentum arteriosum at the isthmus and to the vertebral column by the fascia, it cannot deform as extensively as other locations leading to local stress concentrations. Another reason may be that the aortic wall has an inherently different strength in these locations due to its microstructure, e.g., due to differences in collagen and elastin content, orientation, or cross-linking proteins. Since the  
485 aorta may be subjected to stress concentrations and has heterogeneous strength distributions along the tree, stress and strength are frequently used in models to predict rupture risk. Next we summarize a few existing models designed to evaluate the risk of rupture.

Doyle et al. (2009, 2010) performed inflation tests on silicone rubber to mimic the inflation of abdominal aortic aneurysms (AAA), and observed rupture at the regions of inflections instead of maximum diameter. They also reported rupture at peak stress locations in 80% of the  
490 cases using computational models. Nathan et al. (2011) performed finite element analyses on 47 normal thoracic aortic geometries by assuming that the aortic wall is homogeneous, incompressible, isotropic and linearly elastic, a rather rough assumption. The results showed that the mean wall peak stresses occurred above the sinotubular junction ( $0.43 \pm 0.07$  MPa) and distal  
495 to the left subclavian artery ( $0.21 \pm 0.07$  MPa), which is in line with the common locations of dissection initiation. This led to the conclusion that the stress distribution is the main contributor to the dissection process. Biaxial extension tests on aneurysmatic ( $n = 18$ ) and healthy ( $n = 19$ ) ascending aortic samples showed that aneurysmatic samples are much stiffer under physiological loading conditions (Azadani et al., 2013). Hence, the authors suggested that the

500 patient-specific wall stress could be a good predictor of rupture risk. The study did not find any correlation between the maximum diameter and the patient-specific stress levels. Addressing the large variations in strength and the uncertainties in wall stress predictions, Polzer & Gasser (2015) developed a probabilistic rupture risk index (PRRI), calculated by using the wall strength and the peak stress distribution. The authors were able to distinguish between the intact and ruptured AAA cases. PRRI values were strongly correlated with the mean arterial pressure, 505 but not with the maximum diameter.

On the basis of heterogeneous strength distribution in aneurysm walls, Vallabhaneni et al. (2004) suggested that the locations with increased enzymatic activity within the wall could be responsible for a local weakening making the aneurysm more prone to rupture. Vande Geest et al. (2006b,c) reported different statistical risk prediction models considering the heterogeneity of both the wall stress and the wall strength. Simulations using the model of Vande Geest et al. (2006b) indicated that the unruptured AAAs had significantly higher failure stresses compared to the ruptured group. Even though this model could not be validated by Reeps et al. (2013), it involves a non-invasive estimation of patient-specific wall strength, and it was used 515 by Joldes et al. (2017) to develop a rupture risk calculation software. The approach of Joldes et al. (2017) eliminates the need to use patient-specific material parameters as the stresses are only determined by the external load and the geometry, depending only weakly on the material parameters (for a detailed discussion see Wittek et al. (2009), Miller & Lu (2013) and Joldes et al. (2016)).

520 Trabelsi et al. (2015) compared three different rupture risk assessment methods, in particular, maximum diameter, rupture risk index, and the overpressure index (see definitions therein). The maximum diameter criterion was only weakly correlated with the other two, and, remarkably, the patient with the smallest aneurysm diameter had the highest rupture risk index. Duprey et al. (2016) suggested a rupture risk criterion for aneurysms of ascending aorta based on a maximum stretch parameter  $\gamma_{\text{stretch}}$  the authors introduced. It indicates that the failure is reached 525 when the stretch acting on the tissue is larger than its maximum extensibility. The data obtained via bulge inflation tests therein showed a strong correlation between  $\gamma_{\text{stretch}}$  and the physiological

elastic modulus. Trabelsi et al. (2018) were able to further correlate this rupture risk indicator with the membrane stiffness using the analysis of CT-scans, concluding that the loss of elasticity increases the rupture risk. However, the authors stated that the correlation was not strong enough for this criterion to be suggested for use in clinical practice.

Martin et al. (2013) quantified the rupture diameter risk and the yield diameter risk defined as the diameter  $D_{\text{sys}}$  at systolic pressure divided by the diameter  $D_f$  at rupture pressure ( $D_{\text{sys}}/D_f$ ) and by the diameter  $D_y$  at yield pressure ( $D_{\text{sys}}/D_y$ ), respectively. Both risk indicators were related with increases in the clinically measured parameters such as systolic blood pressure, age, systolic wall tension and pressure-strain modulus (rupture diameter risk was additionally correlated with the aortic size index; for the related definition see Davies et al. (2006)), but not with the aneurysm diameter. Building on this framework, Martin et al. (2015) performed patient-specific finite element analyses using geometries reconstructed from CT scans and clinical blood pressure measurements, in addition to mechanical data from these aortas reported previously by Pham et al. (2013). The rupture diameter risk was correlated with the simulated peak wall stresses and with the tension-strain modulus, but not with the systolic hoop tension and the overall aneurysm diameter. The predicted rupture pressures decreased dramatically with increasing rupture diameter risk.

## 6. Concluding Remarks

Despite the advances in medical, biomedical and biomechanical research, the mortality rates of dissections and aortic aneurysms remain high. The present review article summarizes experimental studies that quantify the aortic wall strength and it discusses biomechanically motivated models to predict rupture risk. Following the description of the aortic microstructure and the pathological changes leading to dissection and aneurysm in Section 2, we summarized experimental investigations that were designed to better understand failure mechanisms involved in dissection and rupture in Section 3. In the case of aortic trauma, we have seen in Section 3.2 that there may be different global load cases on, e.g., the chest resulting in a similar load on the aortic wall leading to a similar material failure. As suggested by Richens et al. (2002), multivariate

555 hypotheses are more suitable to explain under what loading conditions the aorta ruptures. Such hypotheses can bring the global mechanisms together, i.e. shearing, torsion and stretching, and suggest which stresses play a more pronounced role during rupture. Various loads acting on the aortic wall prior to rupture call for the strength identification under different loading modes.

In Section 4 we focused on uniaxial tensile, bulge inflation and peeling tests while briefly touching upon trouser, direct tension and shear tests. We identified contradictory observations and a large variation within and between data sets, which may be due to biological variations, different sample sizes, differences in experimental protocols, etc. However, we pointed to the underlying structural similarities/differences as the main contributor to the similarities/differences of the strength values. Considering the pathological microstructural changes, aneurysmatic and dissected tissues are expected to exhibit different strength properties compared to control tissues although this is not always the case according to the mechanical test results, as pointed out in Section 4. However, it seems that the micro-architecture, in particular the content and organization of collagen and elastin and their cross-linking proteins play an important role during failure.

570 Finally, in Section 5 we looked at what is proposed in the literature to predict the risk of rupture as an alternative to the maximum diameter criterion. Realistic geometries and appropriate constitutive models are crucial to identify wall stresses and zones of stress concentration. Martufi & Gasser (2013) elaborated on a wall-averaged stress state (membrane stress state) to be a more realistic AAA rupture risk indicator, also pointing out the importance of using appropriate constitutive models to predict wall stresses. As mentioned before and addressed by several risk prediction models, not only the stress state at a point in time but also the strength distribution is likely to be heterogeneous. Although rupture risk prediction models address an important issue in clinical practice, they do not model material failure.

Let us finally consider a few more recent findings on tissue failure. Converse et al. (2018) showed that ‘arterial yielding’ was closely correlated with the onset of collagen damage, which is indicated by the binding of collagen hybridizing peptide to undulated collagen (Zitnay et al., 2017). In addition, damage accumulation increased with increasing stretch beyond the ‘yield

threshold', and it occurred primarily in the fibers along the loading direction (Converse et al., 2018). This suggests that orientation and dispersion of collagen determine the strength of, e.g.,  
585 aortic tissues (Sherifova et al., 2019) and the pericardium (Whelan et al., 2019). Marino et al. (2019) proposed a damage model considering interstrand delaminations as a source of inelastic deformation, as suggested by multiscale models of collagen fibrils (Marino & Vairo, 2014; Marino, 2016) and by atomistic computations (Buehler, 2008; Uzel & Buehler, 2011). Employing the experimental protocols documented in Converse et al. (2018), Marino et al. (2019)  
590 showed that damage onset and excessive damage accumulation agree well with the predicted evolution of the model parameters that describe tissue softening associated with permanent molecular elongation, and tissue failure associated with loss of fibril structural integrity.

More advanced failure criteria for fibrous biological tissues are of pressing need to better understand aneurysm rupture and propagation of aortic dissections, and to substantially improve  
595 clinical decision making; should also go hand in hand with developments in clinical biomarkers and/or suitable imaging modalities. In the light of this review, we suggest that an ideal failure criterion should include the strength of the material under different loading cases and the effect of the tissue microstructure on the strength at different length scales. In particular, a failure criterion should be based on microstructural properties including the content and organization  
600 of remodeled collagen and remnant elastin and their cross-linking proteins, especially under the influence of proteolytic activity. Such failure criteria may also improve G&R models necessary of addressing the key issue of rupture-potential.

**Acknowledgement.** We would like to acknowledge Yutaka Nakashima from the Division of Pathology, Japanese Red Cross Fukuoka Hospital in Japan and Justyna A. Niestrawska from  
605 the Institute of Biomechanics, Graz University of Technology in Austria for providing the two images of the microstructure of the aortic dissection and the aneurysm, as presented in the graphical abstract. In addition, we gratefully acknowledge the aneurysm image, also presented in the graphical abstract, which we received from Erasmo Simão da Silva from the Division of Vascular and Endovascular Surgery, University of São Paulo in Brazil and Madhavan L.

610 (Suresh) Raghavan from the Department of Biomedical Engineering, University of Iowa, Iowa City, USA. This work was partly supported by the Lead Project on ‘Mechanics, Modeling and Simulation of Aortic Dissection’, granted by Graz University of Technology, Austria. Furthermore, we gratefully acknowledge the financial support of the National Institutes of Health (NIH), research Grant no. NIH R01HL117063.

615 **References**

- Azadani, A. N., Chitsaz, S., Mannion, A., Mookhoek, A., Wisneski, A., Guccione, J. M., Hope, J. M., Ge, M. D., & Tseng, E. E. (2013). Biomechanical properties of human ascending thoracic aortic aneurysms. *Ann. Thorac. Surg.*, *96*, 50–58.
- van Baardwijk, C., & Roach, M. R. (1987). Factors in the propagation of aortic dissection in  
620 canine thoracic aortas. *J. Biomech.*, *20*, 67–73.
- Ben-Menachem, Y., & Handel, S. (1981). *Angiography in Trauma: A Work Atlas*. WB Saunders.
- Bertrand, S., Cuny, S., Petit, P., Trosseille, X., Page, Y., Guillemot, H., & Drazetic, P. (2008). Traumatic rupture of thoracic aorta in real-world motor vehicle crashes. *Traffic Inj. Prev.*, *9*,  
625 153–161.
- Bode-Jänisch, S., Schmidt, A., Günther, D., Stuhmann, M., & Fieguth, A. (2012). Aortic dissecting aneurysms – histopathological findings. *Forensic. Sci. Int.*, *214*, 13–17.
- Borges, L. F., Blini, J. P. F., Dias, R. R., & Gutierrez, P. S. (2014). Why do aortas cleave or dilate? Clues from an electronic scanning microscopy study in human ascending aortas. *J.*  
630 *Vasc. Res.*, *51*, 50–57.
- Borges, L. F., Jaldin, R. G., Dias, R. R., Stolf, N. A., Michel, J. B., & Gutierrez, P. S. (2008). Collagen is reduced and disrupted in human aneurysms and dissections of ascending aorta. *Hum. Pathol.*, *39*, 437–443.
- Borges, L. F., Touat, Z., Leclercq, A., Zen, A. A., Jondeau, G., Franc, B., Philippe, M., Melihac, O., Gutierrez, P. S., & Michel, J. (2009). Tissue diffusion and retention of metalloproteinases in ascending aortic aneurysms and dissections. *Hum. Pathol.*, *40*, 306–313.  
635
- Brownstein, A. J., Ziganshin, B. A., & Elefteriades, J. A. (2018). Human aortic aneurysm genomic dictionary: is it possible? *Indian J. Thorac. Cardiovasc. Surg.*, doi:10.1007/s12055-018-0659-6.

- 640 Buehler, M. J. (2008). Nanomechanics of collagen fibrils under varying cross-link densities: Atomistic and continuum studies. *J. Mech. Behav. Biomed. Mater.*, *1*, 59–67.
- Campa, J. S., Greenhalgh, R. M., & Powell, J. T. (1987). Elastin degradation in abdominal aortic aneurysms. *Atherosclerosis*, *65*, 13–21.
- Canham, P. B., Finlay, H. M., Dixon, J. G., Boughner, D. R., & Chen, A. (1989). Measurements  
645 from light and polarised light microscopy of human coronary arteries fixed at distending pressure. *Cardiovasc. Res.*, *23*, 973–982.
- Carson, M. W., & Roach, M. R. (1990). The strength of the aortic media and its role in the propagation of aortic dissection. *J. Biomech.*, *23*, 579–588.
- Cherif, H., Gogly, B., Loison-Robert, L.-S., Couty, L., Ferré, F. C., Nassif, A., Lafont, A., &  
650 Fournier, B. P. J. (2015). Comparative study of abdominal and thoracic aortic aneurysms: Their pathogenesis and a gingival fibroblasts-based ex vivo treatment. *Springerplus*, *4*, 231.
- Cheuk, B. L. Y., & Cheng, S. W. K. (2011). Differential expression of elastin assembly genes in patients with Stanford Type A aortic dissection using microarray analysis. *J. Vasc. Surg.*, *53*, 1071–1078.
- 655 Choudhury, N., Bouchot, O., Rouleau, L., Tremblay, D., Cartier, R., Butany, J., Mongrain, R., & Leask, R. L. (2009). Local mechanical and structural properties of healthy and diseased human ascending aorta tissue. *Cardiovasc. Pathol.*, *18*, 83–91.
- Chu, B., Gaillard, E., Mongrain, R., Reiter, S., & Tardif, J. C. (2013). Characterization of fracture toughness exhaustion in pig aorta. *J. Mech. Behav. Biomed. Mater.*, *17*, 126–136.
- 660 Chung, J., Lachapelle, K., Cartier, R., Mongrain, R., & Leask, R. L. (2017). Loss of mechanical directional dependency of the ascending aorta with severe medial degeneration. *Cardiovasc. Pathol.*, *26*, 45–50.

- Chung, J., Lachapelle, K., Wener, E., Cartier, R., De Varennes, B., Fraser, R., & Leask, R. L. (2014). Energy loss, a novel biomechanical parameter, correlates with aortic aneurysm size and histopathologic findings. *J. Thorac. Cardiovasc. Surg.*, *148*, 1082–1089.
- 665
- Cikach, F. S., Koch, C. D., Mead, T. J., Galatioto, J., Willard, B. B., Emerton, K. B., Eagleton, M. J., Blackstone, E. H., Ramirez, F., Roselli, E. E., & Apte, S. S. (2018). Massive aggrecan and versican accumulation in thoracic aortic aneurysm and dissection. *JCI Insight*, *3*, e97167.
- Converse, M. I., Walther, R. G., Ingram, J. T., Li, Y., Yu, S. M., & Monson, K. L. (2018). Detection and characterization of molecular-level collagen damage in overstretched cerebral arteries. *Acta Biomater.*, *67*, 307–318.
- 670
- Crass, J. R., Cohen, A. M., Motta, A. O., Tomashefski Jr, J. F., & Wiesen, E. J. (1990). A proposed new mechanism of traumatic aortic rupture: the osseous pinch. *Radiology*, *176*, 645–649.
- 675
- Creasy, J. D., Chiles, C., Routh, W. D., & Dyer, R. B. (1997). Overview of traumatic injury of the thoracic aorta. *Radiographics*, *17*, 27–45.
- Criado, F. J. (2011). Aortic dissection: a 250-year perspective. *Tex. Heart Inst. J.*, *38*, 694–700.
- Davies, R. R., Gallo, A., Coady, M. A., Tellides, G., Botta, D. M., Burke, B., Coe, M. P., Kopf, G. S., & Elefteriades, J. A. (2006). Novel measurement of relative aortic size predicts rupture of thoracic aortic aneurysms. *Ann. Thorac. Surg.*, *81*, 169–177.
- 680
- Davies, R. R., Goldstein, L. J., Coady, M. A., Tittle, S. L., Rizzo, J. A., Kopf, G. S., & Elefteriades, J. A. (2002). Yearly rupture or dissection rates for thoracic aortic aneurysms: simple prediction based on size. *Ann. Thorac. Surg.*, *73*, 17–27.
- Deveja, R. P., Iliopoulos, D. C., Kritharis, E. P., Angouras, D. C., Sfyris, D., Papadodima, S. A., & Sokolis, D. P. (2018). Effect of aneurysm and bicuspid aortic valve on layer-specific ascending aorta mechanics. *Ann. Thorac. Surg.*, *106*, 1692–1701.
- 685

- Di Martino, E. S., Bohra, A., Vande Geest, J. P., Gupta, N. Y., Makaroun, M. S., & Vorp, D. A. (2006). Biomechanical properties of ruptured versus electively repaired abdominal aortic aneurysm wall tissue. *J. Vasc. Surg.*, *43*, 570–576.
- 690 Dingemans, K. P., Teeling, P., Lagendijk, J. H., & Becker, A. E. (2000). Extracellular matrix of the human aortic media: An ultrastructural histochemical and immunohistochemical study of the adult aortic media. *Anat. Rec.*, *258*, 1–14.
- Doyle, B. J., Cloonan, A. J., Walsh, M. T., Vorp, D. A., & McGloughlin, T. M. (2010). Identification of rupture locations in patient-specific abdominal aortic aneurysms using experimental  
695 and computational techniques. *J. Biomech.*, *43*, 1408–1416.
- Doyle, B. J., Corbett, T. J., Callanan, A., Walsh, M. T., Vorp, D. A., & McGloughlin, T. M. (2009). An experimental and numerical comparison of the rupture locations of an abdominal aortic aneurysm. *J. Endovasc. Ther.*, *16*, 322–335.
- Duprey, A., Trabelsi, O., Vola, M., Favre, J. P., & Avril, S. (2016). Biaxial rupture properties of  
700 ascending thoracic aortic aneurysms. *Acta Biomater.*, *42*, 273–285.
- Elefteriades, J. A. (2008). Thoracic aortic aneurysm: Reading enemy’s playbook. *Yale J. Biol. Med.*, *81*, 175–186.
- Erdheim, J. (1929). Medionecrosis aortae idiopathica. *Virch. Arch. Pathol. Anat.*, *273*, 454–479.
- Ferrara, A., Morganti, S., Totaro, P., Mazzola, A., & Auricchio, F. (2016). Human dilated as-  
705 cending aorta: Mechanical characterization via uniaxial tensile tests. *J. Mech. Behav. Biomed. Mater.*, *53*, 257–271.
- Ferrara, A., Totaro, P., Morganti, S., & Auricchio, F. (2018). Effects of clinico-pathological risk factors on in-vitro mechanical properties of human dilated ascending aorta. *J. Mech. Behav. Biomed. Mater.*, *77*, 1–11.

- 710 Field, M. L., Sastry, P., Zhao, A. R., & Richens, D. (2007). Small vessel avulsion and acute aortic syndrome: A putative aetiology for initiation and propagation of blunt traumatic aortic injury at the isthmus. *Med. Hypotheses*, *68*, 1392–1398.
- Forsell, C., Björck, H. M., Eriksson, P., Franco-Cereceda, A., & Gasser, T. C. (2014). Biomechanical properties of the thoracic aneurysmal wall: Differences between bicuspid aortic  
715 valve and tricuspid aortic valve patients. *Ann. Thorac. Surg.*, *98*, 65–71.
- García-Herrera, C. M., Atienza, J. M., Rojo, F. J., Claes, E., Guinea, G. V., Celentano, D. J., García-Montero, C., & Burgos, R. L. (2012). Mechanical behaviour and rupture of normal and pathological human ascending aortic wall. *Med. Biol. Eng. Comput.*, *50*, 559–566.
- Gasser, T. C., Ogden, R. W., & Holzapfel, G. A. (2006). Hyperelastic modelling of arterial  
720 layers with distributed collagen fibre orientations. *J. R. Soc. Interface*, *3*, 15–35.
- Goldfinger, J. Z., Halperin, J. L., Marin, M. L., Stewart, A. S., Eagle, K. A., & Fuster, V. (2014). Thoracic aortic aneurysm and dissection. *J. Am. Coll. Cardiol.*, *64*, 1725–1739.
- Greenyke, R. M. (1966). Traumatic rupture of aorta. *J. Am. Med. Assoc.*, *195*, 527–530.
- Grootenboer, N., Bosch, J. L., Hendriks, J. M., & van Sambeek, M. R. (2009). Epidemiology,  
725 aetiology, risk of rupture and treatment of abdominal aortic aneurysms: does sex matter? *Eur. J. Vasc. Endovasc. Surg.*, *38*, 278–284.
- Gültekin, O., & Holzapfel, G. A. (2018). A brief review on computational modeling of rupture in soft biological tissues. Computational methods in applied sciences. In O. Oñate, D. Peric, E. de Souza Neto, & M. Chiumenti (Eds.), *Advances in Computational Plasticity. A Book in Honour of D. Roger J. Owen* (pp. 113–144). Springer Nature volume 46.  
730
- Hans, S. S., Jareunpoon, O., Balasubramaniam, M., & Zelenock, G. B. (2005). Size and location of thrombus in intact and ruptured abdominal aortic aneurysms. *J. Vasc. Surg.*, *41*, 584–588.
- Harvey, J. G., & Gough, M. H. (1981). A comparison of the traumatic effects of vascular clamps. *Br. J. Surg.*, *68*, 267–272.

- 735 Haslach, Jr., H. W., Leahy, L. N., Fathi, P., Barrett, J. M., Heyes, A. E., Dumsha, T. A., & McMahon, E. L. (2015). Crack propagation and its shear mechanisms in the bovine descending aorta. *Cardiovasc. Eng. Technol.*, *6*, 501–518.
- Haslach, Jr., H. W., Riley, P., & Molotsky, A. (2011). The influence of medial substructures on rupture in bovine aortas. *Cardiovasc. Eng. Technol.*, *2*, 372–387.
- 740 Haslach, Jr., H. W., Siddiqui, A., Weerasooriya, A., Nguyen, R., Roshgadol, J., Monforte, N., & McMahon, E. (2018). Fracture mechanics of shear crack propagation and dissection in the healthy bovine descending aortic media. *Acta Biomater.*, *68*, 53–66.
- Helpenstein-Didier, C., Taïnoff, D., Viville, J., Adrien, J., Maire, É., & Badel, P. (2018). Tensile rupture of medial arterial tissue studied by X-ray micro-tomography on stained samples. *J. Mech. Behav. Biomed. Mater.*, *78*, 362–368.
- 745 Henson, G. F., & Rob, C. G. (1956). A comparative study of the effects of different arterial clamps on the vessel wall. *Br. J. Surg.*, *43*, 561–564.
- Holzappel, G. A., & Fereidoonzhad, B. (2017). Modeling of damage in soft biological tissues. In Y. Payan, & J. Ohayon (Eds.), *Biomechanics of Living Organs. Hyperelastic Constitutive*  
750 *Laws for Finite Element Modeling* (pp. 101–123). Academic Press.
- Holzappel, G. A., Gasser, T. C., & Ogden, R. W. (2000). A new constitutive framework for arterial wall mechanics and a comparative study of material models. *J. Elasticity*, *61*, 1–48.
- Humphrey, J. D., & Holzappel, G. A. (2012). Mechanics, mechanobiology, and modeling of human abdominal aorta and aneurysms. *J. Biomech.*, *45*, 805–814.
- 755 Iliopoulos, D. C., Deveja, R. P., Kritharis, E. P., Perrea, D., Sionis, G. D., Toutouzas, K., Stefanadis, C., & Sokolis, D. P. (2009a). Regional and directional variations in the mechanical properties of ascending thoracic aortic aneurysms. *Med. Eng. Phys.*, *31*, 1–9.

- Iliopoulos, D. C., Kritharis, E. P., Giagini, A. T., Papadodima, S. A., & Sokolis, D. P. (2009b). Ascending thoracic aortic aneurysms are associated with compositional remodeling and vessel stiffening but not weakening in age-matched subjects. *J. Thorac. Cardiovasc. Surg.*, *137*, 101–109.
- Isselbacher, E. M. (2005). Thoracic and abdominal aortic aneurysms. *Circulation*, *111*, 816–828.
- Jameson, J. L., Fauci, A. S., Kasper, D. L., Hauser, S. L., Longo, D. L., & Loscalzo, J. (2018). *Harrison's Principle of Internal Medicine*. (20th ed.). McGraw-Hill Education.
- Joldes, G. R., Miller, K., Wittek, A., & Doyle, B. (2016). A simple, effective and clinically applicable method to compute abdominal aortic aneurysm wall stress. *J. Mech. Behav. Biomed. Mater.*, *58*, 139–148.
- Joldes, G. R., Miller, K., Wittek, A., Forsythe, R., Newby, D. E., & Doyle, B. J. (2017). BioPARR: A software system for estimating the rupture potential index for abdominal aortic aneurysms. *Sci. Rep.*, *7*, 4641.
- Jones, J. A., Beck, C., Barbour, J. R., Zavadzkas, J. A., Mukherjee, R., Spinale, F. G., & Ikonomidis, J. S. (2009). Alterations in aortic cellular constituents during thoracic aortic aneurysm development: myofibroblast-mediated vascular remodeling. *Am. J. Pathol.*, *175*, 1746–1756.
- Keen, G. (1972). Closed injuries of the thoracic aorta. *Ann. Roy. Coll. Surg. Engl.*, *51*, 137–156.
- Kim, J., Staiculescu, M. C., Cocciolone, A. J., Yanagisawa, H., Mecham, R. P., & Wagenseil, J. E. (2017). Crosslinked elastic fibers are necessary for low energy loss in the ascending aorta. *J. Biomech.*, *61*, 199–207.
- Kim, J. H., Avril, S., Duprey, A., & Favre, J. P. (2012). Experimental characterization of rupture in human aortic aneurysms using a full-field measurement technique. *Biomech. Model. Mechanobiol.*, *11*, 841–853.

- Kivity, Y., & Collins, R. (1974). Nonlinear wave propagation in viscoelastic tubes: Application to aortic rupture. *J. Biomech.*, 7, 67–76.
- 785 Kożuń, M. (2016). Delamination properties of the human thoracic arterial wall with early stage of atherosclerosis lesions. *J. Theor. Appl. Mech.*, 54, 229–238.
- Kożuń, M., Kobielarz, M., Chwiłkowska, A., & Pezowicz, C. (2018). The impact of development of atherosclerosis on delamination resistance of the thoracic aortic wall. *J. Mech. Behav. Biomed. Mater.*, 79, 292–300.
- 790 Kritharis, E. P., Iliopoulos, D. C., Papadodima, S. A., & Sokolis, D. P. (2014). Effects of aneurysm on the mechanical properties and histologic structure of aortic sinuses. *Ann. Thorac. Surg.*, 98, 72–79.
- Lederle, F. A., Wilson, S. E., Johnson, G. R., Reinke, D. B., Littooy, F. N., Acher, C. W., Ballard, D. J., Messina, L. M., Gordon, I. L., Chute, E. P., Krupski, W. C., Busuttil, S. J.,  
795 Barone, G. W., Sparks, S., Graham, L. M., Rapp, J. H., Makaroun, M. S., Moneta, G. L., Cambria, R. A., Makhoul, R. G., Eton, D., Ansel, H. J., Freischlag, J. A., Bandyk, D., & Aneurysm Detection and Management Veterans Affairs Cooperative Study Group (2002). Immediate repair compared with surveillance of small abdominal aortic aneurysms. *N. Engl. J. Med.*, 346, 1437–1444.
- 800 Luo, Y., Duprey, A., Avril, A., & Lu, J. (2016). Characteristics of thoracic aortic aneurysm rupture in vitro. *Acta Biomater.*, 42, 286–295.
- MacLean, N. F., Dudek, N. L., & Roach, M. R. (1999). The role of radial elastic properties in the development of aortic dissections. *J. Vasc. Surg.*, 29, 703–710.
- Manopoulos, C., Karathanasis, I., Kouerinis, I., Angouras, D. C., Lazaris, A., Tsangaris, S.,  
805 & Sokolis, D. P. (2018). Identification of regional/layer differences in failure properties and thickness as important biomechanical factors responsible for the initiation of aortic dissections. *J. Biomech.*, 80, 102–110.

- Marino, M. (2016). Molecular and intermolecular effects in collagen fibril mechanics: a multi-scale analytical model compared with atomistic and experimental studies. *Biomech. Model. Mechanobiol.*, *15*, 133–154.
- 810
- Marino, M., Converse, M. I., Monson, K. L., & Wriggers, P. (2019). Molecular-level collagen damage explains softening and failure of arterial tissues: A quantitative interpretation of CHP data with a novel elasto-damage model. *J. Mech. Behav. Biomed. Mater.*, *97*, 254–271.
- Marino, M., & Vairo, G. (2014). Influence of inter-molecular interactions on the elasto-damage mechanics of collagen fibrils: A bottom-up approach towards macroscopic tissue modeling. *J. Mech. Phys. Solids*, *73*, 38–54.
- 815
- Marra, S. P., Kennedy, F. E., Kinkaid, J. N., & Fillinger, M. F. (2006). Elastic and rupture properties of porcine aortic tissue measured using inflation testing. *Cardiovasc. Eng.*, *6*, 125–133.
- 820
- Marsh, C. L., & Moore, R. C. (1957). Deceleration trauma. *Am. J. Surg.*, *93*, 623–631.
- Marshall, T. K. (1958). Traumatic dissecting aneurysms. *J. Clin. Pathol.*, *11*, 36–39.
- Martin, C., Sun, W., & Elefteriades, J. (2015). Patient-specific finite element analysis of ascending aorta aneurysms. *Am. J. Physiol. Heart Circ. Physiol.*, *308*, H1306–H1316.
- Martin, C., Sun, W., Pham, T., & Elefteriades, J. (2013). Predictive biomechanical analysis of ascending aortic aneurysm rupture potential. *Acta Biomater.*, *9*, 9392–9400.
- 825
- Martufi, G., & Gasser, T. C. (2013). Review: the role of biomechanical modeling in the rupture risk assessment for abdominal aortic aneurysms. *J. Biomech. Eng.*, *135*, 021010.
- Martufi, G., Satriano, A., Moore, R. D., Vorp, D. A., & Di Martino, E. S. (2015). Local quantification of wall thickness and intraluminal thrombus offer insight into the mechanical properties of the aneurysmal aorta. *Ann. Biomed. Eng.*, *43*, 1759–1771.
- 830
- Mikich, M. (2003). Dissection of the aorta: a new approach. *Heart*, *89*, 6–8.

- Miller, K., & Lu, J. (2013). On the prospect of patient-specific biomechanics without patient-specific properties of tissues. *J. Mech. Behav. Biomed. Mater.*, *27*, 154–166.
- Mohan, D., & Melvin, J. W. (1982). Failure properties of passive human aortic tissue. I –  
835 uniaxial tension tests. *J. Biomech.*, *15*, 887–902.
- Mohan, D., & Melvin, J. W. (1983). Failure properties of passive human aortic tissue. II –  
biaxial tension tests. *J. Biomech.*, *16*, 31–44.
- Nakashima, Y. (2010). Pathogenesis of aortic dissection: Elastic fiber abnormalities and aortic  
medial weakness. *Ann. Vasc. Dis.*, *3*, 28–36.
- 840 Nathan, D. P., Xu, C., Gorman III, J. H., Fairman, R. M., Bavaria, J. E., Gorman, R. C., Chan-  
dran, K. B., & Jackson, B. M. (2011). Pathogenesis of acute aortic dissection: A finite  
element stress analysis. *Ann. Thorac. Surg.*, *91*, 458–463.
- Niestrawska, J. A., Viertler, C., Regitnig, P., Cohnert, T. U., Sommer, G., & Holzapfel, G. A.  
(2016). Microstructure and mechanics of healthy and aneurysmatic abdominal aortas: exper-  
845 imental analysis and modeling. *J. R. Soc. Interface*, *13*, 20160620.
- Noble, C., Smulders, N., Lewis, R., Carré, M. J., Franklin, S. E., MacNeil, S., & Taylor, T. A.  
(2016). Controlled peel testing of a model tissue for diseased aorta. *J. Biomech.*, *49*, 3667–  
3675.
- Oberwalder, P. J. (2001). Aneurysmen und Dissektionen der thorakalen Aorten: Definition und  
850 Pathologie. *J. Kardiol.*, *8*, 2–4.
- Okamoto, R. J., Wagenseil, J. E., DeLong, W. R., Peterson, S. J., Kouchoukos, N. T., & Sundt,  
T. M. (2002). Mechanical properties of dilated human ascending aorta. *Ann. Biomed. Eng.*,  
*30*, 624–635.
- Olsson, C., Thelin, S., Sthle, E., Ekbom, A., & Granath, F. (2006). Thoracic aortic aneurysm  
855 and dissection: increasing prevalence and improved outcomes reported in a nationwide

population-based study of more than 14,000 cases from 1987 to 2002. *Circulation*, *114*, 2611–2618.

O’Connell, M. K., Murthy, S., Phan, S., Xu, C., Buchanan, J., Spilker, R., Dalman, R. L., Zarins, C. K., Denk, W., & Taylor, C. A. (2008). The three-dimensional micro- and nanostructure of the aortic medial lamellar unit measured using 3D confocal and electron microscopy imaging. *Matrix Biol.*, *27*, 171–181.

O’Leary, S. A., Mulvihill, J. J., Barrett, H. E., Kavanagh, E. G., Walsh, M. T., McGloughlin, T., & Doyle, B. J. (2015). Determining the influence of calcification on the failure properties of abdominal aortic aneurysm (aaa) tissue. *J. Mech. Behav. Biomed. Mater.*, *42*, 154 – 167.

Pal, S., Tsamis, A., Pasta, S., D’Amore, A., Gleason, T. G., Vorp, D. A., & Maiti, S. (2014). A mechanistic model on the role of radially-running collagen fibers on dissection properties of human ascending thoracic aorta. *J. Biomech.*, *47*, 981–988.

Pape, L. A., Awais, M., Woznicki, E. M., Suzuki, T., Trimarchi, S., Evangelista, A., Myrmel, T., Larsen, M., Harris, K. M., Greason, K., Di Eusanio Bossone, M., Montgomery, D. G., Eagle, K. A., Nienaber, C. A., Isselbacher, E. M., & O’Gara, P. (2015). Presentation, diagnosis, and outcomes of acute aortic dissection: 17-year trends from the international registry of acute aortic dissection. *J. Am. Coll. Cardiol.*, *66*, 350–358.

Pape, L. A., Tsai, T. T., Isselbacher, E. M., Oh, J. K., O’Gara, P. T., Evangelista, A., Fattori, R., Meinhardt, G., Trimarchi, S., Bossone, E., Suzuki, T., Cooper, J. V., Froehlich, J. B., Nienaber, C. A., Eagle, K. A., & International Registry of Acute Aortic Dissection (IRAD) Investigators (2007). Aortic diameter  $\geq$  5.5 cm is not a good predictor of type A aortic dissection: Observations from the International Registry of Acute Aortic Dissection (IRAD). *Circulation*, *116*, 1120–1127.

Pasta, S., Phillippi, J. A., Gleason, T. G., & Vorp, D. A. (2012). Effect of aneurysm on the mechanical dissection properties of the human ascending thoracic aorta. *J. Thorac. Cardiovasc. Surg.*, *143*, 460–467.

- Pearson, R., Philips, N., Hancock, R., Hashim, S., Field, M., Richens, D., & McNally, D. (2008). Regional wall mechanics and blunt traumatic aortic rupture at the isthmus. *Eur. J. Cardiothorac. Surg.*, *34*, 616–622.
- 885 Peterss, S., Mansour, A. M., Ross, J. A., Vaitkeviciute, I., Charilaou, P., Dumfarth, J., Fang, H., Ziganshin, B. A., Rizzo, J. A., Adeniran, A. J., & Elefteriades, J. A. (2016). Changing pathology of the thoracic aorta from acute to chronic dissection: Literature review and insights. *J. Am. Coll. Cardiol.*, *68*, 1054–1065.
- Pham, T., Martin, C., Elefteriades, J., & Sun, W. (2013). Biomechanical characterization of  
890 ascending aortic aneurysm with concomitant bicuspid aortic valve and bovine aortic arch. *Acta Biomater.*, *9*, 7927–7936.
- Phillippi, J. A., Green, B. R., Eskay, M. A., Kotlarczyk, M. P., Hill, M. R., Robertson, A. M., Watkins, S. C., Vorp, D. A., & Gleason, T. G. (2014). Mechanism of aortic medial matrix remodeling is distinct in patients with bicuspid aortic valve. *J. Thorac. Cardiovasc. Surg.*,  
895 *147*, 1056–1064.
- Pichamuthu, J. E., Phillippi, J. A., Cleary, D. A., Chew, D. W., Hempel, J., Vorp, D. A., & Gleason, T. G. (2013). Differential tensile strength and collagen composition in ascending aortic aneurysms by aortic valve phenotype. *Ann. Thorac. Surg.*, *96*, 2147–2154.
- Polzer, S., & Gasser, C. T. (2015). Biomechanical rupture risk assessment of abdominal aortic  
900 aneurysms based on a novel probabilistic rupture risk index. *J. R. Soc. Interface*, *12*, 20150852.
- Prijon, T., & Ermenc, B. (2010). Classification of blunt aortic injuries a new systematic overview of aortic trauma. *Forensic. Sci. Int.*, *195*, 6–9.
- Purslow, P. P. (1983). Positional variations in fracture toughness, stiffness and strength of  
905 descending thoracic pig aorta. *J. Biomech.*, *16*, 947–953.

- Raghavan, M. L., Hanaoka, M. M., Kratzberg, J. A., de Lourdes Higuchi, M., & da Silva, E. S. (2011). Biomechanical failure properties and microstructural content of ruptured and unruptured abdominal aortic aneurysms. *J. Biomech.*, *44*, 2501–2507.
- 910 Raghavan, M. L., Kratzberg, J., Castro de Tolosa, E. M., Hanaoka, M. M., Walker, P., & da Silva, E. S. (2006). Regional distribution of wall thickness and failure properties of human abdominal aortic aneurysm. *J. Biomech.*, *39*, 3010–3016.
- Raghavan, M. L., Webster, M. W., & Vorp, D. A. (1996). Ex vivo biomechanical behavior of abdominal aortic aneurysm: assesment using a new mathematical model. *Ann. Biomed. Eng.*, *24*, 573–582.
- 915 Rajagopal, K., Bridges, C., & Rajagopal, K. R. (2007). Towards an understanding of the mechanics underlying aortic dissection. *Biomech. Model. Mechanobiol.*, *6*, 345–359.
- Reeps, C., Maier, A., Pelisek, J., Härtl, F., Grabher-Meier, V., Wall, W. A., Essler, M., Eckstein, H. H., & Gee, M. W. (2013). Measuring and modeling patient-specific distributions of material properties in abdominal aortic aneurysm wall. *Biomech. Model. Mechanobiol.*, *12*,  
920 717–733.
- Richens, D., Field, M., Neale, M., & Oakley, C. (2002). Review: The mechanism of injury in blunt traumatic rupture of the aorta. *Eur. J. Cardio-thorac.*, *21*, 288–293.
- Roach, M. R., & Song, S. H. (1994). Variations in strength of the porcine aorta as a function of location. *Clin. Invest. Med.*, *17*, 308–318.
- 925 Romo, A., Badel, P., Duprey, A., Favre, J. P., & Avril, S. (2014). In vitro analysis of localized aneurysm rupture. *J. Biomech.*, *47*, 607–616.
- Ruddy, J. M., Jones, J. A., & Ikonomidis, J. S. (2013). Pathophysiology of thoracic aortic aneurysm (TAA): is it not one uniform aorta? Role of embryologic origin. *Prog. Cardiovasc. Dis.*, *56*, 68–73.

- 930 Saeyeldin, A. A., Velasquez, C. A., Mahmood, S. U. B., Brownstein, A. J., Zafar, M. A., Zigan-  
ganshin, B. A., & Elefteriades, J. A. (2017). Thoracic aortic aneurysm: unlocking the “silent  
killer” secrets. *Gen. Thorac. Cardiovasc. Surg.*, *67*, 1–11.
- Sassani, S. G., Tsangaris, S., & Sokolis, D. P. (2015). Layer- and region-specific material  
characterization of ascending thoracic aortic aneurysms by microstructure-based models. *J.*  
935 *Biomech.*, *48*, 3757–3765.
- Schermerhorn, M. (2009). A 66-year-old man with an abdominal aortic aneurysm: review of  
screening and treatment. *J. Am. Med. Assoc.*, *302*, 2015–2022.
- Schriebl, A. J., Zeindlinger, G., Pierce, D. M., Regitnig, P., & Holzapfel, G. A. (2012). Deter-  
mination of the layer-specific distributed collagen fiber orientations in human thoracic and  
940 abdominal aortas and common iliac arteries. *J. R. Soc. Interface*, *9*, 1275–1286.
- Sevitt, S. (1977). The mechanisms of traumatic rupture of the thoracic aorta. *Br. J. Surg.*, *64*,  
166–173.
- Shah, S. B., Witzenburg, C., Hadi, M. F., Wagner, H. P., Goodrich, J. M., Alford, P. W., &  
Barocas, V. H. (2014). Prefailure and failure mechanics of the porcine ascending thoracic  
945 aorta: experiments and a multiscale model. *J. Biomech. Eng.*, *136*, 021028–1.
- Shahmansouri, N., Alreshidan, M., Emmott, A., Lachapelle, K., Cartier, R., Leask, R. L., &  
Mongrain, R. (2016). Evaluating ascending aortic aneurysm tissue toughness: Dependence  
on collagen and elastin contents. *J. Mech. Behav. Biomed. Mater.*, *64*, 262 – 271.
- Sherifova, S., Sommer, G., Viertler, C., Regitnig, P., Caranasos, T., Smith, M. A., Griffith,  
950 B. E., Ogden, R. W., & Holzapfel, G. A. (2019). Failure properties and microstructure of  
healthy and aneurysmatic human thoracic aortas with a focus on the media. *Acta Biomater.*,  
submitted.
- Shimizu, K., Mitchell, R. N., & Libby, P. (2006). Inflammation and cellular immune responses  
in abdominal aortic aneurysms. *Arterioscler. Thromb. Vasc. Biol.*, *26*, 987–994.

- 955 Shkrum, M. J., McClafferty, K. J., Green, R. N., Nowak, E. S., & Young, J. G. (1999). Mechanisms of aortic injury in fatalities occurring in motor vehicle collisions. *J. Forensic Sci.*, *44*, 44–56.
- Sokolis, D. P., & Iliopoulos, D. C. (2014). Impaired mechanics and matrix metalloproteinases/inhibitors expression in female ascending thoracic aortic aneurysms. *J. Mech. Behav. Biomed. Mater.*, *34*, 154–164.
- 960 Sokolis, D. P., Kritharis, E. P., Giagini, A. T., Lampropoulos, K. M., Papadodima, S. A., & Iliopoulos, D. C. (2012a). Biomechanical response of ascending thoracic aortic aneurysms: association with structural remodelling. *Comput. Methods Biomech. Biomed. Engin.*, *15*, 231–248.
- 965 Sokolis, D. P., Kritharis, E. P., & Iliopoulos, D. C. (2012b). Effect of layer heterogeneity on the biomechanical properties of ascending thoracic aortic aneurysms. *Med. Biol. Eng. Comput.*, *50*, 1227–1237.
- Sommer, G., Gasser, T. C., Regitnig, P., Auer, M., & Holzapfel, G. A. (2008). Dissection properties of the human aortic media: an experimental study. *J. Biomech. Eng.*, *130*, 021007–1–12.
- 970 Sommer, G., Sherifova, S., Oberwalder, P. J., Dapunt, O. E., Ursomanno, P. A., DeAnda, A., Griffith, B. E., & Holzapfel, G. A. (2016). Mechanical strength of aneurysmatic and dissected human thoracic aortas at different shear loading modes. *J. Biomech.*, *49*, 2374–2382.
- Soyer, R., Bessou, J. P., Bouchart, F., Tabley, A., Mouton-Schleifer, D., Arrignon, J., & Redonnet, M. (1992). Acute traumatic isthmic aortic rupture: Long-term results in 49 patients. *Eur. J. Cardiothorac. Surg.*, *6*, 431–437.
- 975 Stry, H. C. (2003). *Atlas of Atherosclerosis: Progression and Regression*. (2nd ed.). Boca Raton, London, New York, Washington, D.C.: The Parthenon Publishing Group.

- Sugita, S., & Matsumoto, T. (2013a). Heterogeneity of deformation of aortic wall at the microscopic level: Contribution of heterogeneous distribution of collagen fibers in the wall. *Biomed. Mater. Eng.*, *23*, 447–461.
- Sugita, S., & Matsumoto, T. (2013b). Novel biaxial tensile test for studying aortic failure phenomena at a microscopic level. *Biomed. Eng. Online*, *12*:3.
- Sugita, S., & Matsumoto, T. (2018). Local distribution of collagen fibers determines crack initiation site and its propagation direction during aortic rupture. *Biomech. Model. Mechanobiol.*, *17*, 577–587.
- Sugita, S., Matsumoto, T., Ohashi, T., Kumagai, K., Akimoto, H., Tabayashi, K., & Sato, M. (2012). Evaluation of rupture properties of thoracic aortic aneurysms in a pressure-imposed test for rupture risk estimation. *Cardiovascular Engineering and Technology*, *3*, 41–51.
- Svensson, L. G., Kouchoukos, N. T., Miller, D. C., Bavaria, J. E., Coselli, J. S., Curi, M. A., Eggebrecht, H., Elefteriades, J. A., Erbel, R., Gleason, T. G., Lytle, B. W., Mitchell, R. S., Nienaber, C. A., Roselli, E. E., Safi, H. J., Shemin, R. J., Sicard, G. A., Sundt 3rd, T. M., Szeto, W. Y., Wheatley 3rd, G. H., & Society of Thoracic Surgeons Endovascular Surgery Task Force (2008). Expert consensus document on the treatment of descending thoracic aortic disease using endovascular stent-grafts. *Ann. Thorac. Surg.*, *85*, S1–S41.
- Tam, A. S. M., Sapp, M. C., & Roach, M. R. (1998). The effect of tear depth on the propagation of aortic dissections in isolated porcine thoracic aorta. *J. Biomech.*, *31*, 673–676.
- Thubrikar, M. J., Labrosse, M., Robicsek, F., Al-Soudi, J., & Fowler, B. (2001). Mechanical properties of abdominal aortic aneurysm wall. *J. Med. Eng. Technol.*, *25*, 133–142.
- Tiessen, I. M., & Roach, M. R. (1993). Factors in the initiation and propagation of aortic dissections in human autopsy aortas. *J. Biomech. Eng.*, *115*, 123–125.

- Tong, J., Cheng, Y., & Holzapfel, G. A. (2016). Mechanical assessment of arterial dissection in health and disease: Advancements and challenges. *J. Biomech.*, *49*, 2366–2373.
- 1005 Tong, J., Cohnert, T., Regitnig, P., Kohlbacher, J., Birner-Gruenberger, R., Schriebl, A. J., Sommer, G., & Holzapfel, G. A. (2014). Variations of dissection properties and mass fractions with thrombus age in human abdominal aortic aneurysms. *J. Biomech.*, *47*, 14–23.
- Trabelsi, O., Davis, F. M., Rodriguez-Matas, J. F., Duprey, A., & Avril, S. (2015). Patient specific stress and rupture analysis of ascending thoracic aneurysms. *J. Biomech.*, *48*, 1836–  
1010 1843.
- Trabelsi, O., Gutierrez, M., Farzaneh, S., Duprey, A., & Avril, S. (2018). A non-invasive methodology for ATAA rupture risk estimation. *J. Biomech.*, *66*, 119–126.
- Tsamis, A., Phillippi, J. A., Koch, R. G., Chan, P. G., Krawiec, J. T., D’Amore, A., Watkins, S. C., Wagner, W. R., Vorp, D. A., & Gleason, T. G. (2016). Extracellular matrix fiber  
1015 microarchitecture is region-specific in bicuspid aortic valve-associated ascending aortopathy. *J. Thorac. Cardiovasc. Surg.*, *151*, 1718–1728.e5.
- Tsamis, A., Phillippi, J. A., Koch, R. G., Pasta, S., D’Amore, A., Watkins, S. C., Wagner, W. R., Gleason, T. G., & Vorp, D. A. (2013). Fiber micro-architecture in the longitudinal-radial and circumferential-radial planes of ascending thoracic aortic aneurysm media. *J. Biomech.*, *46*,  
1020 2787–2794.
- Uzel, S. G. M., & Buehler, M. J. (2011). Molecular structure, mechanical behavior and failure mechanism of the C-terminal cross-link domain in type I collagen. *J. Mech. Behav. Biomed. Mater.*, *4*, 153–161.
- Vallabhaneni, S. R., Gilling-Smith, G. L., How, T. V., Carter, S. D., Brennan, J. A., & Harris, P. L. (2004). Heterogeneity of tensile strength and matrix metalloproteinase activity in the  
1025 wall of abdominal aortic aneurysms. *J. Endovasc. Ther.*, *11*, 494–502.

- Vande Geest, J. P., Dillavou, E. D., Di Martino, E. S., Oberdier, M., Bohra, A., Makaroun, M. S., & Vorp, D. A. (2006a). Gender-related differences in the tensile strength of abdominal aortic aneurysm. *Ann. N.Y. Acad. Sci.*, *1085*, 400–402.
- 1030 Vande Geest, J. P., Di Martino, E. S., Bohra, A., Makaroun, M. S., & Vorp, D. A. (2006b). A biomechanics-based rupture potential index for abdominal aortic aneurysm risk assessment: demonstrative application. *Ann. N. Y. Acad. Sci.*, *1085*, 11–21.
- Vande Geest, J. P., Wang, D. H. J., Wisniewski, S. R., Makaroun, M. S., & Vorp, D. A. (2006c). Towards a noninvasive method for determination of patient-specific wall strength distribution  
1035 in abdominal aortic aneurysms. *Ann. Biomed. Eng.*, *34*, 1098–1106.
- Viano, D. (1983). Biomechanics of nonpenetrating aortic trauma: a review. *SAE Technical Paper 831608*, (pp. 109–114).
- Vorp, D. A. (2007). Biomechanics of abdominal aortic aneurysm. *J. Biomech.*, *40*, 1887–1902.
- Vorp, D. A., Lee, P. C., Wang, D. H., Makaroun, M. S., Nemoto, E. M., Ogawa, S., & Webster,  
1040 M. W. (2001). Association of intraluminal thrombus in abdominal aortic aneurysm with local hypoxia and wall weakening. *J. Vasc. Surg.*, *34*, 291–299.
- Vorp, D. A., Raghavan, M. L., Muluk, S. C., Makaroun, M. S., Steed, D. L., Shapiro, R., & Webster, M. W. (1996). Wall strength and stiffness of aneurysmal and nonaneurysmal abdominal aorta. *Ann. N.Y. Acad. Sci.*, *800*, 274–276.
- 1045 Vorp, D. A., Schiro, B. J., Ehrlich, M. P., Juvonen, T. S., Ergin, M. A., & Griffith, B. P. (2003). Effect of aneurysm on the tensile strength and biomechanical behavior of the ascending thoracic aorta. *Ann. Thorac. Surg.*, *800*, 1210–1214.
- Wang, L., Zhang, J., Fu, W., Guo, D., Jiang, J., & Wang, Y. (2012). Association of smooth muscle cell phenotypes with extracellular matrix disorders in thoracic aortic dissection. *J.*  
1050 *Vasc. Surg.*, *56*, 1698–1709.

- Wang, X., LeMaire, S. A., Chen, L., Shen, Y. H., Gan, Y., Bartsch, H., Carter, S. A., Utama, B.,  
Ou, H., Coselli, J. S., & Wang, X. L. (2006). Increased collagen deposition and elevated ex-  
pression of connective tissue growth factor in human thoracic aortic dissection. *Circulation*,  
*114*, I-200–I-205.
- 1055 Whelan, A., Duffy, J., Gaul, R. T., O'Reilly, D., Nolan, D. R., Gunning, P., Lally, C., & Mur-  
phy, B. P. (2019). Collagen fibre orientation and dispersion govern ultimate tensile strength,  
stiffness and the fatigue performance of bovine pericardium. *J. Mech. Behav. Biomed. Mater.*,  
*90*, 54–60.
- Wilson, H., & Roome, N. W. (1933). Traumatic shock syndrome following rupture of the aorta  
1060 and multiple fractures. *Am. J. Surg.*, *23*, 333.
- Wittek, A., Hawkins, T., & Miller, K. (2009). On the unimportance of constitutive models in  
computing brain deformation for image-guided surgery. *Biomech. Model. Mechanobiol.*, *8*,  
77–84.
- Witzenburg, C. M., Dhume, R. Y., Shah, S. B., Korenczuk, C. E., Wagner, H. P., Alford, P. W.,  
1065 & Barocas, V. H. (2017). Failure of the porcine ascending aorta: multidirectional experiments  
and a unifying microstructural model. *J. Biomech. Eng.*, *139*, 031005–031005–14.
- Wolinsky, H. (1970). Comparison of medial growth of human thoracic and abdominal aortas.  
*Circ. Res.*, *27*, 531–538.
- Wolinsky, H., & Glagov, S. (1967). A lamellar unit of aortic medial structure and function in  
1070 mammals. *Circ. Res.*, *20*, 90–111.
- Wolinsky, H., & Glagov, S. (1969). Comparison of abdominal and thoracic aortic medial struc-  
ture in mammals. deviation of man from the usual pattern. *Circ. Res.*, *25*, 677–686.
- Wu, D., Shen, Y. H., Russell, L., Coselli, J. S., & LeMaire, S. A. (2013). Molecular mechanisms  
of thoracic aortic dissection. *J. Surg. Res.*, *184*, 907–924.

1075 Xiong, J., Wang, S. M., Zhou, W., & Wu, J. G. (2008). Measurement and analysis of ultimate mechanical properties, stress-strain curve fit, and elastic modulus formula of human abdominal aortic aneurysm and nonaneurysmal abdominal aorta. *J. Vasc. Surg.*, *48*, 189–195.

Zehnder, M. A. (1956). Delayed post-traumatic rupture of the aorta in a young healthy individual after closed injury; mechanical-etiological considerations. *Angiology*, *7*, 252–267.

1080 Zitnay, J. L., Li, Y., Qin, Z., San, B. H., Depalle, B., Reese, S. P., Buehler, M. J., Yu, S. M., & Weiss, J. A. (2017). Molecular level detection and localization of mechanical damage in collagen enabled by collagen hybridizing peptides. *Nat. Commun.*, *8*, 14913.

Table 1: Overview of uniaxial tensile test results on aortas – tests performed until failure: ABA, abdominal aorta; AN, aneurysmatic; ASA, ascending aorta; BAV, bicuspid aortic valve; Circ, circumferential; DTA, descending thoracic aorta; H, healthy; Long, longitudinal; TAV, tricuspid aortic valve; <sup>+</sup> values for stress; \* values for extension.

Study	Species	Location	Healthy/ Diseased	Additional information	Direction	<i>n</i>	Failure stress (kPa)	Failure stretch (–)
Mohan & Melvin (1982)	Human	DTA	H	Quasi-static	Circ	18	1720 ± 890	1.23 ± 0.28
					Long	18	1470 ± 910	1.47 ± 0.23
				Dynamic	Circ	16 <sup>+</sup> , 17*	5070 ± 3290	1.60 ± 0.28
					Long	18 <sup>+</sup> , 21*	3590 ± 2040	1.64 ± 0.28
Raghavan et al. (1996)	Human	ABA	H	–	Long	7	2014 ± 394	–
			AN	–	Circ	16	1019 ± 160	–
Vorp et al. (2001)	Human	ABA	AN	ILT > 4 mm ILT < 4 mm	Long	45	864 ± 102	–
					Circ	7	1380 ± 190	–
Vorp et al. (2003)	Human	ASA	H	–	Circ	7	1800 ± 240	–
					Long	7	1710 ± 140	–
Di Martino et al. (2006)	Human	ABA	AN	Ruptured Unruptured	Circ	23	1180 ± 120	–
					Circ	17	1210 ± 90	–
					Circ	13	540 ± 60	–
Vande Geest et al. (2006c)	Human	ABA	AN	For model input	Circ	26	820 ± 90	–
					Circ	60	805 ± 60	–
García-Herrera et al. (2012)	Human	ASA	H	For validation < 35 yrs	Circ	21	832 ± 85	–
					Circ	–	2180 ± 240	2.35 ± 0.1
					Long	–	1140 ± 100	2.00 ± 0.1
					Circ	–	1200 ± 200	–
				AN	Long	–	660 ± 70	–
					Circ	–	1230 ± 150	1.80 ± 0.08
					Long	–	840 ± 100	1.58 ± 0.06
					Circ	–	1190 ± 130	–
Pichamuthu et al. (2013)	Human	ASA	AN	BAV	Circ	–	880 ± 120	–
					Long	–	880 ± 120	–
				TAV	Circ	–	1656 ± 98	1.92 ± 0.04
					Long	–	698 ± 31	1.63 ± 0.02
Shah et al. (2014)	Porcine	ASA	–	–	Circ	–	961 ± 61	1.61 ± 0.04
					Long	–	540 ± 37	1.47 ± 0.03
Ferrara et al. (2016)	Human	ASA	AN	Anterior	Circ	11	2510 ± 439.3	1.99 ± 0.07
					Long	11	750 ± 102.6	1.92 ± 0.16
Sommer et al. (2016)	Human	ASA	AN	Posterior	Circ	37	1440 ± 700	1.35 ± 0.16
					Long	34	940 ± 490	1.34 ± 0.15
				Media	Circ	32	1850 ± 700	1.36 ± 0.12
					Long	19	740 ± 180	1.31 ± 0.09
Sommer et al. (2016)	Human	ASA	AN	Media	Circ	7	1282 ± 822	1.52 ± 0.20
					Long	10	565 ± 198	1.52 ± 0.18

Table 2: Overview of bulge inflation test results on aortas: AN, aneurysmatic; ASA, ascending aorta; Circ, circumferential; DTA, descending thoracic aorta; Long, longitudinal; TA, thoracic aorta; <sup>a</sup> Laplace stress; <sup>b</sup> stress perpendicular to the crack direction; <sup>c</sup> mean stretch; <sup>d</sup> circumferential stretch; <sup>e</sup> average Green–Lagrange strain; <sup>f</sup> stretch perpendicular to the crack direction.

Study	Species	Location	Healthy/ Diseased	Speed (mm/min)	Additional information	Direction	<i>n</i>	Failure stress (kPa)	Failure extension (–)	
Marra et al. (2006)	Porcine	TA	–	60	–	Long	25	1750 ± 710	1.523 ± 0.178 <sup>c</sup>	
Pearson et al. (2008)	Porcine	ASA	–	–	–	–	10	3699 ± 789	1.85 ± 0.114 <sup>d</sup>	
		DTA	–	–	–	–	10	4260 ± 1626	1.70 ± 0.138 <sup>d</sup>	
		Isthmus	–	–	–	–	10	3248 ± 1430	1.66 ± 0.109 <sup>d</sup>	
		ASA	AN	15	Media	Circ	6	547.5 ± 362.6	0.192 ± 0.08 <sup>e</sup>	
Kim et al. (2012)	Human	ASA	AN	15	Media	Long	6	335.3 ± 103.8	0.261 ± 0.117 <sup>e</sup>	
						Adventitia	Circ	3	636.6 ± 322.7	0.252 ± 0.091 <sup>e</sup>
						Long	3	976 ± 247.2	0.343 ± 0.123 <sup>e</sup>	
Sugita et al. (2012)	Porcine	TA	–	15	Proximal	–	6	1810 ± 430 <sup>a</sup>	–	
					Distal	–	6	2290 ± 740 <sup>a</sup>	–	
Romo et al. (2014)	Human	TA	AN	–	–	–	6	980 ± 390 <sup>a</sup>	–	
	Human	ASA	AN	15	Media	–	9	780 ± 200 <sup>b</sup>	–	
Duprey et al. (2016)	Human	ASA	AN	15	Adventitia	–	6	1460 ± 103 <sup>b</sup>	–	
					Composite	–	31	1260 ± 940 <sup>b</sup>	1.37 ± 0.15 <sup>f</sup>	

Table 3: Overview of peeling test results on aortas: A, adventitia; ABA, abdominal aorta; Age\*, age of intraluminal thrombus; AM, adventitia + media; AN, aneurysmatic; AT, atherosclerosis; ASA, ascending aorta; BAV, bicuspid aortic valve; Circ, circumferential;  $F/w$ , force per width; Long, longitudinal; H, healthy; MI, media + intima; TA, thoracic aorta; TAV, tricuspid aortic valve;  $W_{\text{diss}}$ , dissection energy; + according to Stary (2003).

Study	Species	Location	Healthy/ Diseased	Additional information	Direction	$n$	$F/w$ (mN/mm)	$W_{\text{diss}}$ (mJ/cm <sup>2</sup> )				
Sommer et al. (2008)	Human	ABA	H	Media	Circ	5	22.9 ± 2.9	5.1 ± 0.6				
					Long	7	34.8 ± 15.5	7.6 ± 2.7				
Pasta et al. (2012)	Human	ASA	H	Control	Circ	7	126 ± 6.6	–				
					Long	7	149 ± 7.6	–				
					AN	TAV	Circ	8	109.1 ± 5.2	–		
							Long	8	116.8 ± 6.1	–		
					BAV	Circ	16	88.4 ± 4.1	–			
						Long	16	100 ± 4.1	–			
Tong et al. (2014)	Human	ABA	AN	Age* II, A	Circ	11	–	10.1 ± 1.7				
					Long	9	–	9.3 ± 0.9				
				Age* III, A	Circ	8	–	9.2 ± 2.0				
					Long	7	–	8.3 ± 1.3				
				Age* IV, A	Circ	6	–	8.6 ± 1.4				
					Long	7	–	7.8 ± 1.0				
				Age* II, MI	Circ	12	–	6.7 ± 1.2				
					Long	12	–	8.4 ± 1.9				
				Age* III, MI	Circ	8	–	5.5 ± 1.1				
					Long	8	–	6.8 ± 1.7				
				Age* IV, MI	Circ	7	–	4.2 ± 1.1				
					Long	6	–	5.1 ± 1.4				
				Kozuń (2016)	Human	TA	AT (stage II <sup>+</sup> )	A–MI	Circ	26	24.5 ± 7.5	5.6 ± 0.9
									Long	7	32.4 ± 6.5	7.6 ± 1.7
AM–I	Circ	22	26.5 ± 6.7					4.1 ± 1.0				
	Long	8	34.2 ± 3.5					4.7 ± 0.9				
Noble et al. (2016)	Porcine	TA	–	Control	Circ	16	67.4 ± 11.7	15.18 ± 2.70				
					Long	16	76.7 ± 25.9	18.33 ± 6.42				
				Collagenase	Circ	17	49.3 ± 11.9	10.81 ± 2.80				
					Long	14	53.9 ± 12.2	13.58 ± 3.12				
				Elastase	Circ	16	58.8 ± 17.3	13.24 ± 4.00				
					Long	14	69.1 ± 27.0	17.18 ± 7.12				
				Glutaraldehyde treatment	Circ	13	91.2 ± 28.2	19.01 ± 6.05				
					Long	14	83.6 ± 13.7	18.63 ± 3.35				

## Legend of Figures:

**Figure 1:** (a) Anatomy of the aorta with some of its branches; (b) sketch of a dissected wall  
1085 with arrows indicating the blood flow.

**Figure 2:** Structure of the aorta: (a) healthy but aged aortic wall with non-atherosclerotic intimal thickening composed of three layers – intima (I), media (M) and adventitia (A). Reprinted with permission from Gasser et al. (2006); (b) layered collagen architecture of a healthy and aged abdominal aorta – more specifically the top image depicts the out-of-plane structure in the  
1090 circumferential-radial plane, while the three images at the bottom show in-plane sections of the intima (I), media (M) and adventitia (A) (white scale bars corresponding to  $100\mu\text{m}$ . Adapted from Niestrawska et al. (2016); (c) 3D microstructure of an aortic media consisting of several lamellar units – circumferentially-oriented radially-tilted smooth muscle cells (SMCs) with elliptical nuclei (N) sandwiched between elastic lamellas (EL) surrounded by a dense network of  
1095 interlamellar elastin fibers (IEFs shown with black arrows), elastin struts (ES), and reinforced elastin pores (EP). Reprinted with permission from O’Connell et al. (2008); (d) schematic representation of two SMCs and two fenestrated EL with their interconnections – more specifically, collagen fibers (Coll) are closely associated with EL, surface ridges of the left SMC are connected to both EL via elastin protrusions, right SMC is connected to the lower EL via oxytalan  
1100 fiber (Ox), and larger deposits (D) containing collagen and heparan sulfate proteoglycan are found at indentations of the cell surface. Reprinted with permission from Dingemans et al. (2000).

**Figure 3:** Microstructural changes due to pathological formations in human thoracic aortas with stars indicating mucoïd accumulation areas (proteoglycan pools): (a),(b) disorganized collagen  
1105 network visualized by (a) a histological section stained by picrosirius – collagen framework is disorganized – and (b) scanning electron microscopy (SEM); (c),(d) SEM images showing a lamellar structure disrupted probably by the proteoglycan pools (star) (Adv = Adventitia; End = endothelium coverage of the luminal face). Reprinted with permission from Borges et al. (2014); (e),(f) histological sections stained by Alcian blue showing (e) a pathological aorta with

1110 areas of mucoid accumulations (stars) – inset shows immunostaining for  $\alpha$ -actin demonstrat-  
ing the absence of SMCs inside the mucoid area; (f) control aorta where the space between  
elastic lamellae (arrow) is occupied by SMCs, collagen, and a normal amount of mucoid sub-  
stance (light blue). Adapted from Borges et al. (2009); (g),(h) SEM images depicting the elastic  
fiber architecture of human aortic medias from (g) an aortic dissection patient and (h) a control  
1115 subject (black scale bars indicate  $20\mu\text{m}$ . Reprinted with permission from Nakashima (2010).

**Figure 4:** Pressure volume curves to create a bleb in the thoracic and abdominal sections of the  
aorta. Reprinted with permission from Roach & Song (1994).

**Figure 5:** Initiation/propagation of aortic dissections due to shear stresses: (a)–(c) cracks vis-  
ible after a block shear test, where the white areas are openings in the tissue. Reprinted with  
1120 permission from Haslach, Jr. et al. (2015); (a),(b) are slices in the circumferential-longitudinal  
plane where the horizontal direction is longitudinal – (a) circumferential deformation parallel to  
the collagen fibers and (b) longitudinal deformation; (c) slice in the radial-circumferential plane  
after circumferential deformation, where the horizontal direction is circumferential; (d) cracks  
visible as black zones between the lamellae in the radial-circumferential plane after an in-plane  
1125 shear test in the circumferential direction. Adapted from Sommer et al. (2016); (e) cracks that  
occurred during a uniaxial test indicated by black arrows. Reprinted with permission from  
Helfenstein-Didier et al. (2018).

**Figure 6:** Aortic dissection and rupture due to traumatic injury. Adapted from Prijon & Er-  
menc (2010): (a) case presenting multiple ruptures: intramural and transmural, latter both in  
1130 circumferential and longitudinal directions indicated by white arrows; (b) intramural rupture of  
the intima; (c) intramural rupture of the intima and the media.

**Figure 7:** Experimental tests typically used to quantify the failure properties of aortas: (a) bone-  
shaped specimen for a uniaxial tensile test with load  $F$ ; (b) bulge inflation test with pressure  
load  $p$ ; (c) peeling test; (d) trouser test, as used in, e.g., Purslow (1983); (e) direct tension test

1135 to quantify radial strength, as used in, e.g., Sommer et al. (2008, 2016); (f) in-plane shear test with the sheared plane indicated in gray, as used in, e.g., Sommer et al. (2016). Black arrows and dashed lines indicate the load direction and the incision, respectively. Tests (a),(c),(d) and (f) can be performed in any tissue direction in the tangential plane.

**Figure 8:** Stress-strain data of ascending thoracic aortic aneurysm (ATAA) and control specimens taken from the anterior region with (a) circumferential and (b) longitudinal orientation obtained from uniaxial tensile tests. Data show a large variability in failure properties. Reprinted with permission from Iliopoulos et al. (2009b).

**Figure 9:** Histological images (Elastica van Gieson) of the dissection tips obtained from a peeling test of an aortic media during peeling in (a) circumferential and (b) longitudinal directions. Reprinted with permission from Sommer et al. (2008). The images highlight the irreversible mechanism of the separation at the microscopic level. (c) Schematic of fiber bridging failure; the matrix is already separated but still connected by an unruptured fiber (above); force–separation law ( $F$  vs  $\Delta$ ) for a collagen fiber bridge with nonlinear loading and linear post peak behavior starting at  $F_{\max}$  and related  $\Delta_p$  (below) – modes of fiber deformation and failure are depicted in the insets. Shaded region represents the energy  $U_f$  required for failure of the fiber bridge. Adapted from Pal et al. (2014).

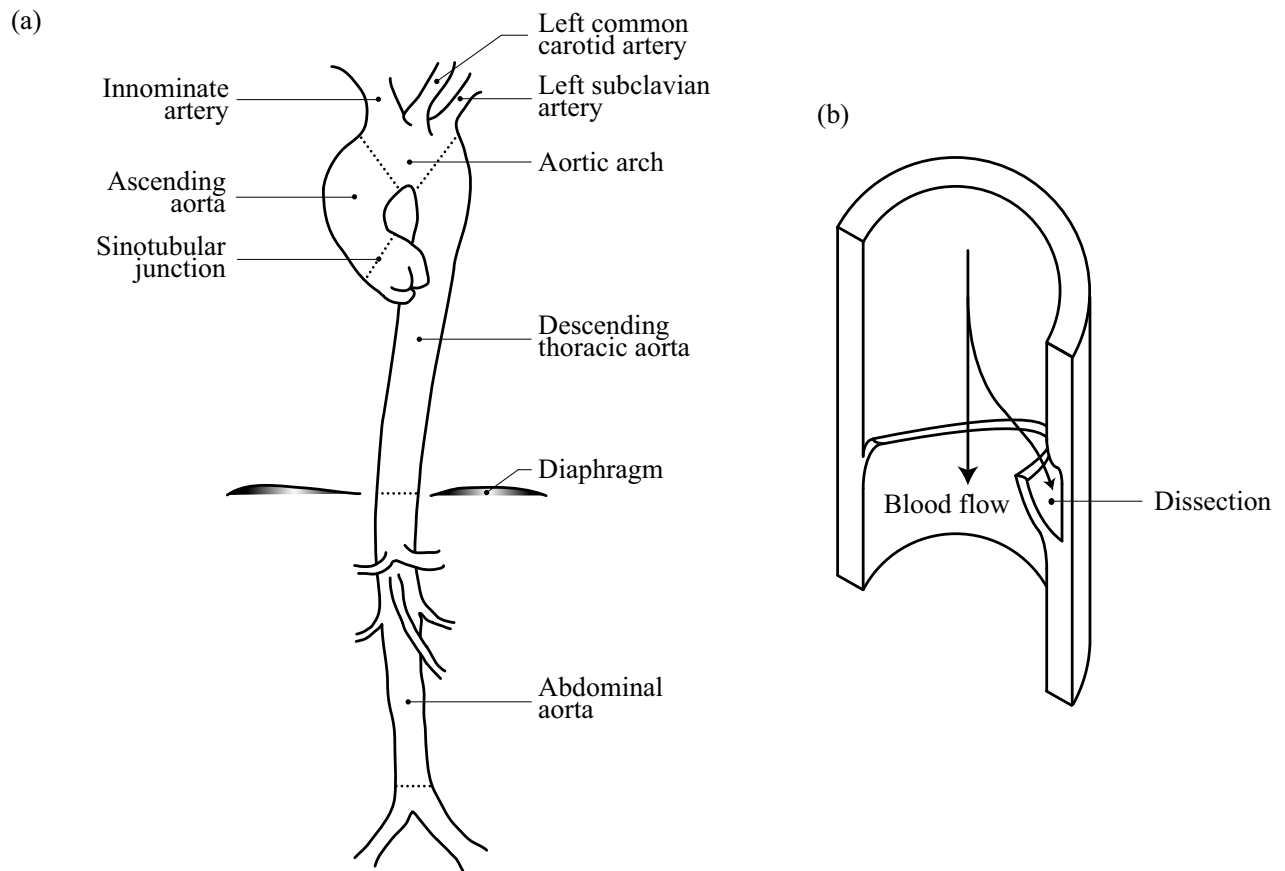


Figure 1

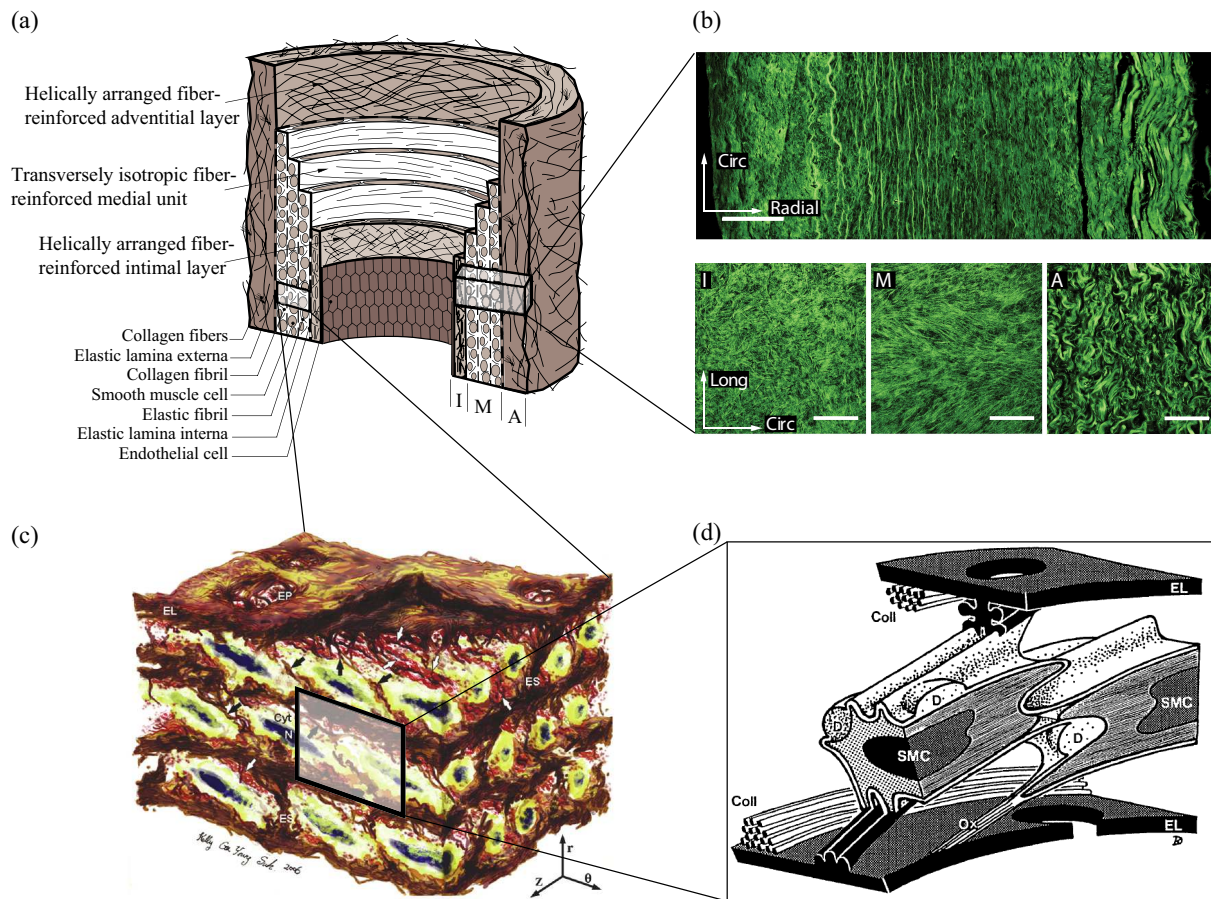


Figure 2

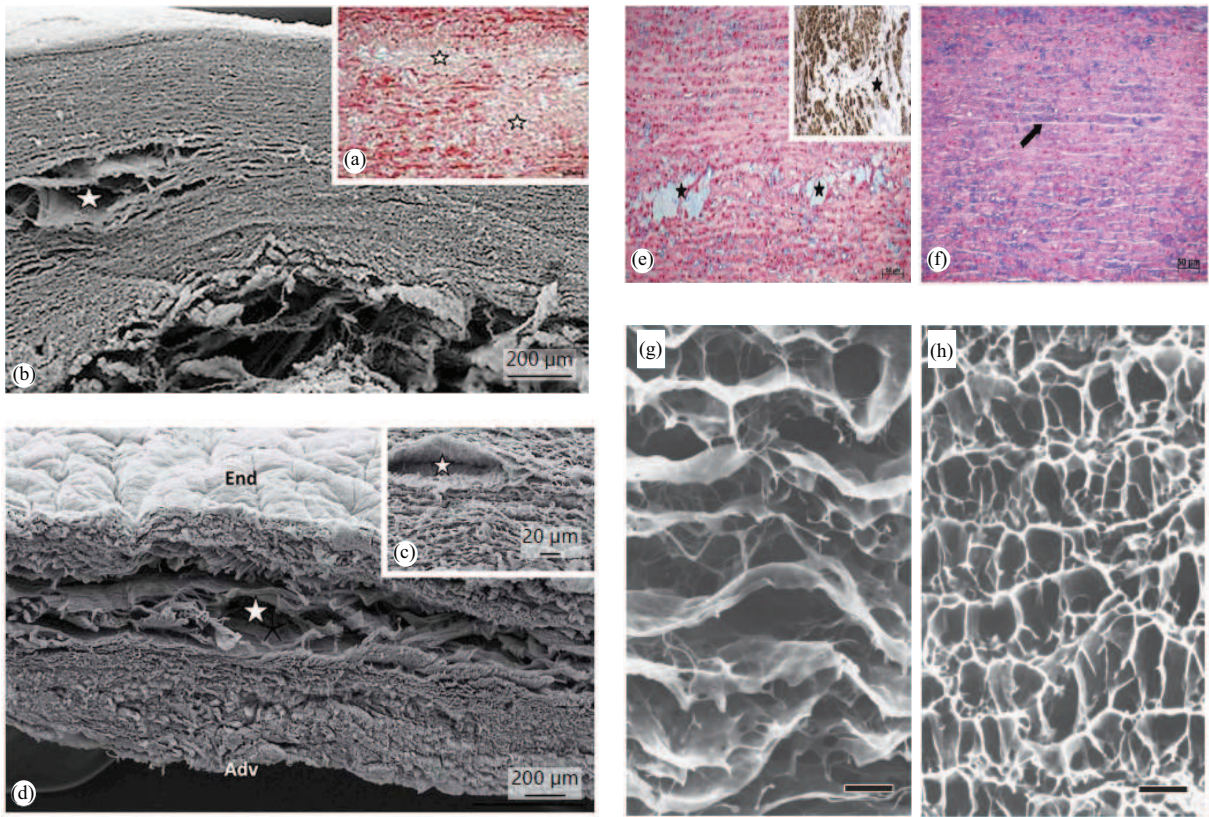


Figure 3

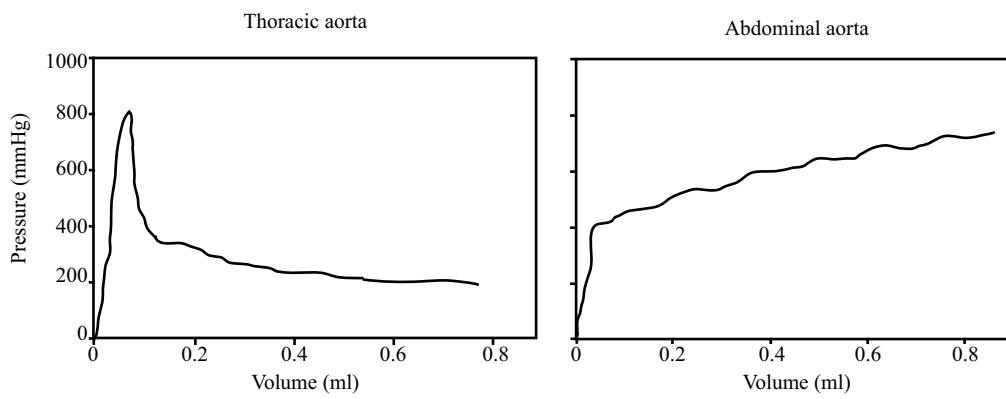


Figure 4

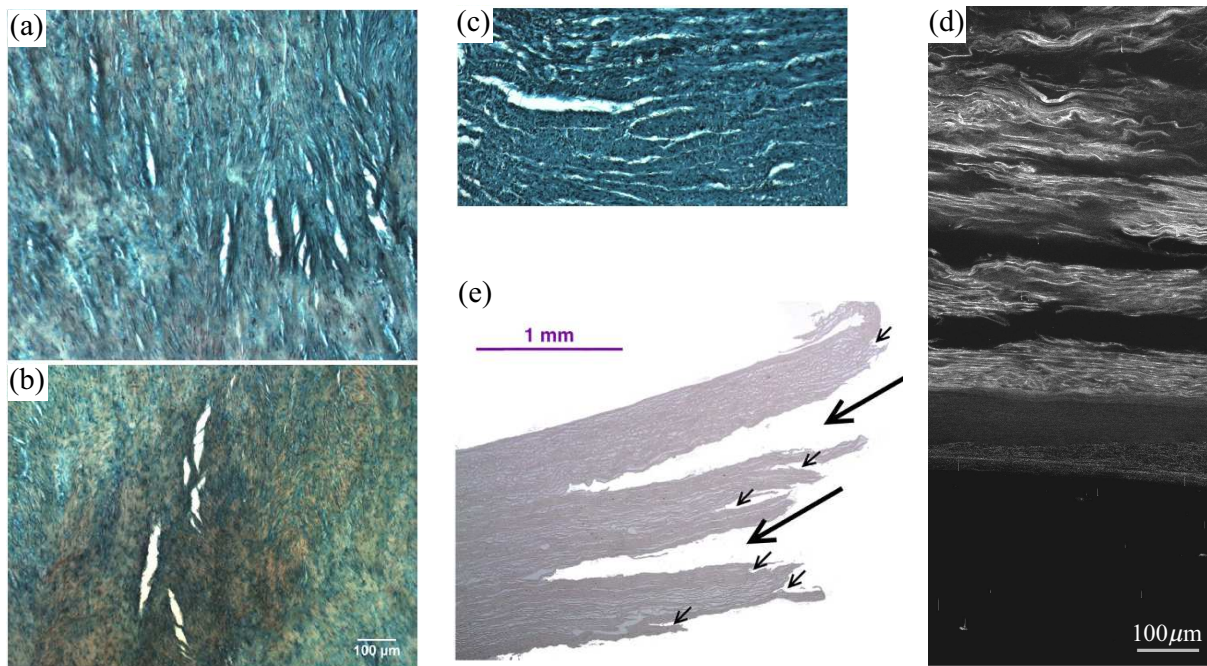


Figure 5

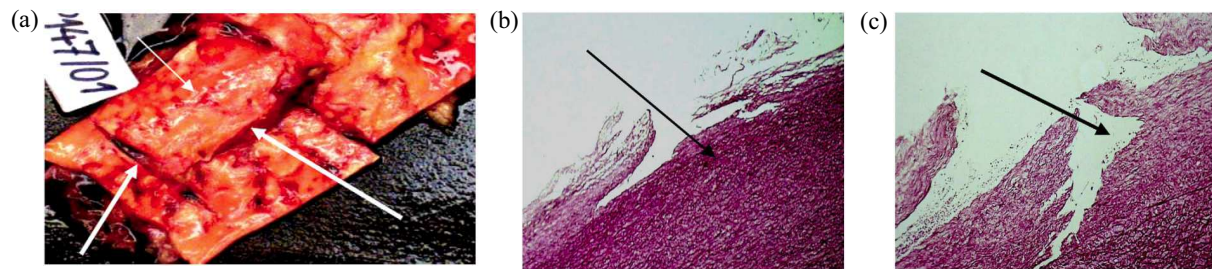
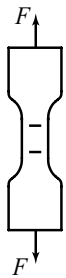
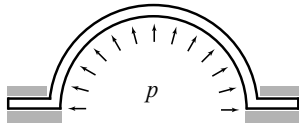


Figure 6

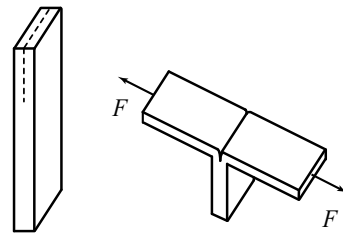
(a) Uniaxial tensile test



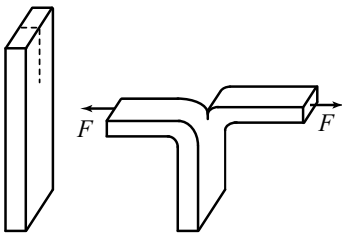
(b) Bulge inflation test



(c) Peeling test



(d) Trouser test



(e) Direct tension test



(f) In-plane shear test

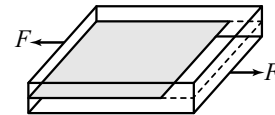


Figure 7

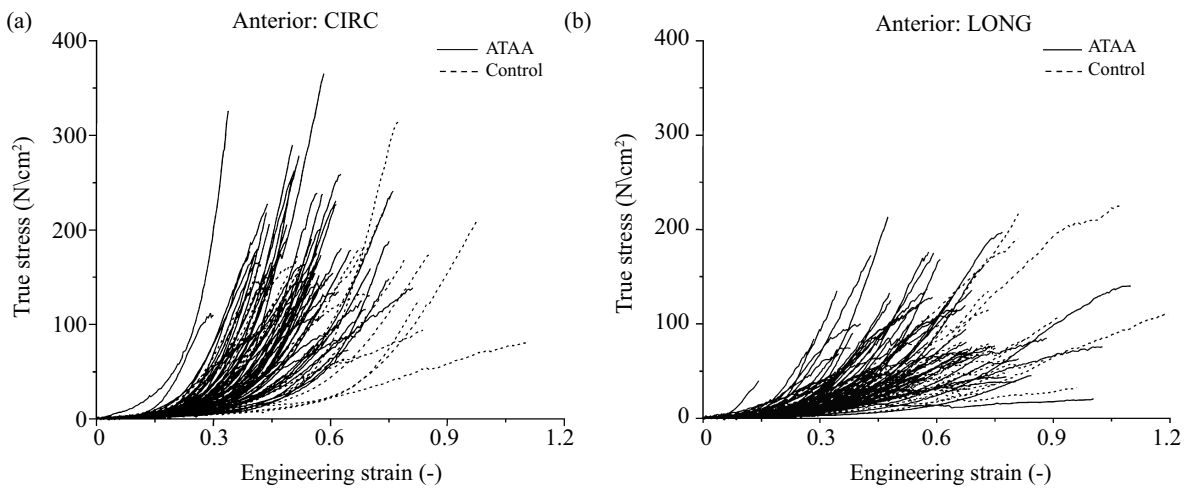


Figure 8

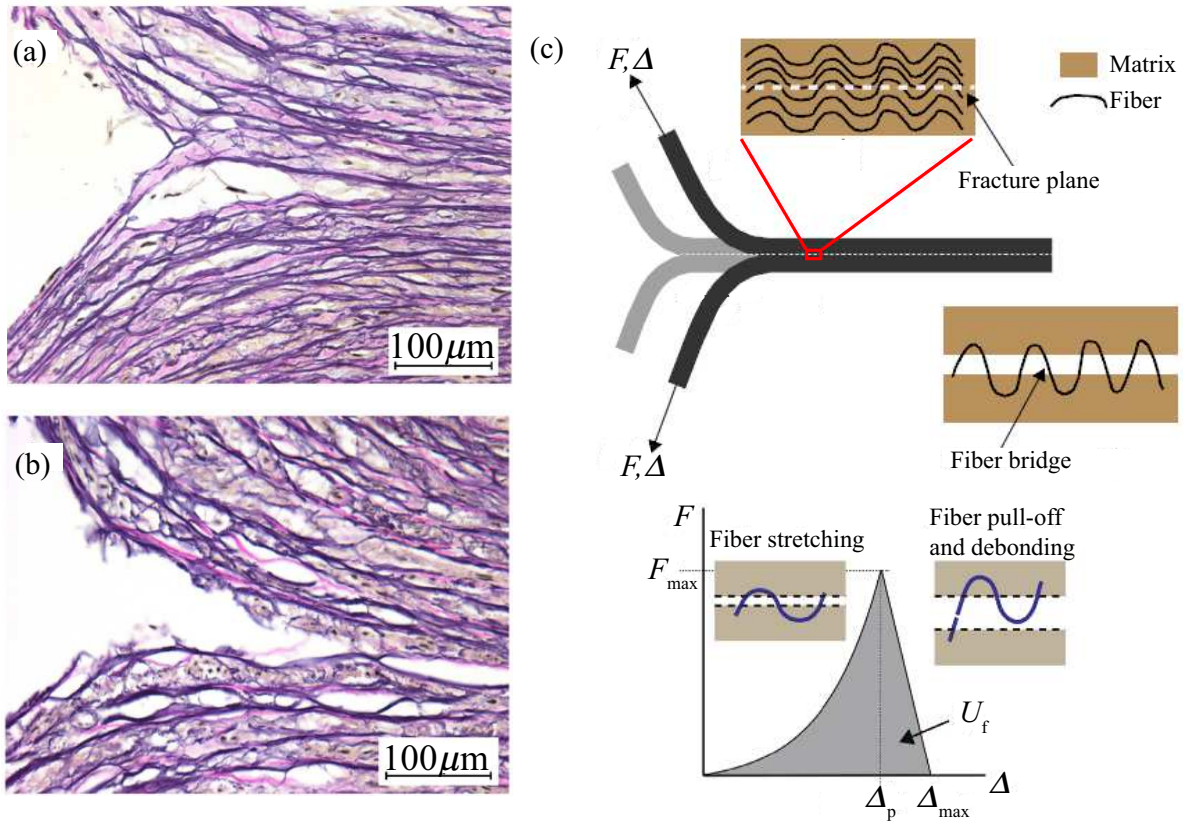


Figure 9